T H E U N I V E R S I T Y O F M I C H I G A N

COLLEGE OF ENGINEERING
Department of Nuclear Engineering
Radiation-Solid-State Physics Laboratory

Progress Report

STUDY OF MICROWAVE, RADIOFREQUENCIES, AND IONIZING RADIATION INTERACTIONS IN SOLIDS

C. Kikuchi
R. Borcherts
N. Mahootian
I. Chen
R. Oswald, Jr.

ORA Project 04381

under contract with:

NATIONAL AERONAUTICS AND SPACE ADMINISTRATION
OFFICE OF SPACE SCIENCES
CONTRACT NO. NsG-115-61
WASHINGTON, D.C.

administered through:

OFFICE OF RESEARCH ADMINISTRATION ANN ARBOR

February 1963

TABLE OF CONTENTS

LIST OF TABLES

LIST OF FIGURES

Part C

PART A

VANADIUM SOLID-STATE CHEMISTRY BY PARAMAGNETIC RESONANCE

by

C. Kikuchi, R. Borcherts and N. Mahootian

I. INTRODUCTION

It is very well known by now that electron spin resonance, besides having applications to masers,[1] has proved and is continuing to prove useful as a research tool. In the early days of paramagnetic resonance, this phenomenon was used to determine nuclear spins, magnetic moments,[2] and electric quadrupole moments.[3] Later it was used to determine the nature of electron wave functions in organic molecules[4] to study the symmetry properties of the crystalline electric field in which the paramagnetic ion is embedded,[5,6] and more recently a suggestion has been made that detailed information about the nature of local distortions in crystals can be obtained by means of the electron spin resonance technique.[7]

The specific aspect of electron spin resonance that will be discussed here is the use of this technique to determine the oxidation states of paramagnetic impurities in crystalline solids, with particular emphasis on the changes in such chemical states brought about by ionizing radiations. To illustrate the general procedure, we will limit the discussion to vanadium. Our interest in vanadium stems from the fact that it is essentially isotopically pure V^{51} (V^{51}, 99.75%; V^{50}, 0.25%) whose nuclear spin is 7/2, so that vanadium has an easily recognizable paramagnetic resonance signature; and also from the fact that the different valence states of vanadium can be produced within a particular host crystal with relative ease. In this respect, vanadium is different from manganese, which has been used in electron spin resonance studies concerned with the divalent manganous ion.

This program in vanadium solid-state chemistry stemmed from our study of V^{2+}, V^{3+}, and V^{4+} in vanadium sapphire.[8] As mentioned in that paper, we were unable to provide the details of certain electron transfer processes that took place as a result of X-ray irradiation. In order to obtain some insight to the mechanisms involved, we turned our attention to a systematic study of the vanadyl, VO^{++}, and the vanadous, V^{++}, ions in the Tutton salts,[9] and more recently have initiated some studies on vanadium in polycrystalline samples, such as in MgO and Al_2O_3 powders. Consequently, we shall here review the results of our study of vanadium in sapphire, discuss the properties of vanadium in Tutton salts, and then mention some of the preliminary results of our studies of vanadium in powders.

II. VANADIUM SAPPHIRE

To illustrate the ESR techniques used to determine valence states, consider first vanadium sapphire. As indicated above, one characteristic of vanadium is that it has a readily recognizable paramagnetic resonance signature—8 hyperfine structure (hfs) lines. The electron configuration and electron spin states of vanadium for the different valence states are as follows:

Ion	Electron Configuration	Electron Spin
V^{4+}	$3d$	1/2
V^{3+}	$3d^2$	1
V^{2+}	$3d^3$	3/2

Each of the above vanadium valence states gives rise to an ESR absorption spectrum with a definite number of groups of 8 hfs lines, and each group has a characteristic angular dependence.

Consider first V^{4+}. The electron spin is 1/2, so that the ESR absorption spectrum should consist of a single group of 8 lines. The ESR spectrum of this vanadium state in sapphire is shown in Fig. 1. The lines are very weak. The spectrum seems to be isotropic, with $g = 1.97$ and $A = B = 1.32 \times 10^{-4} cm^{-1}$. This spectrum was observed in vanadium sapphire prepared from a powder mixture containing 0.1% vanadium pentoxide.

Consider next V^{3+}. Vanadium in sapphire is considered to be in Al^{3+} substitutional sites; V^{3+} in corundum was first observed by Zverev and Prok-

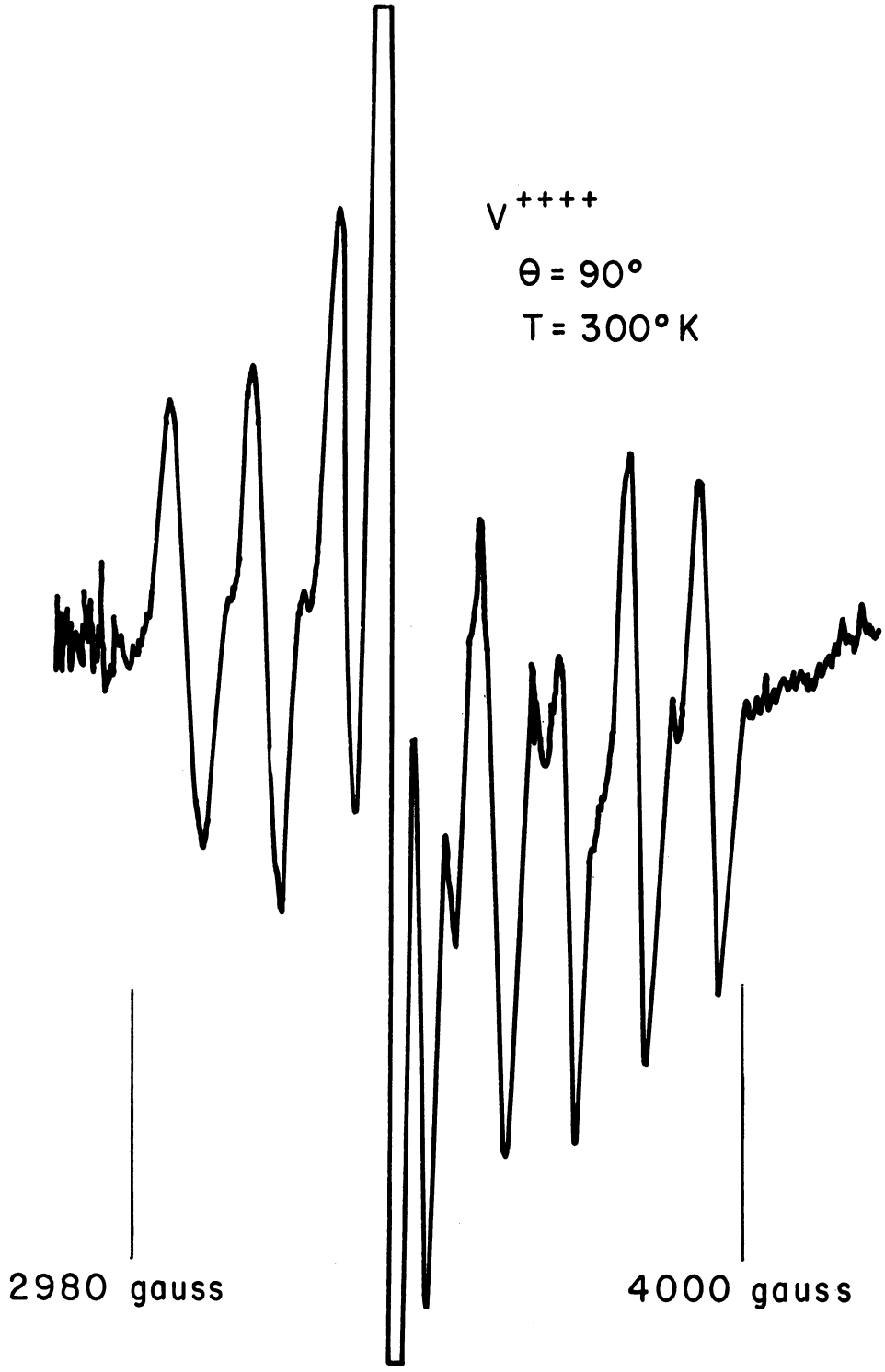

Fig. 1. ESR spectrum of V^{4+} in sapphire.

horov,[10] and their ESR results constitute a confirmation of the detections from magnetic susceptibility measurements by Siegert[11] and by van der Handel and Siegert.[12] Further confirmatory optical investigations have been reported by Pryce and Runciman.[13]

Theory and experiment indicate that the V^{3+} ground state, whose spin is 1, consists of two levels, one for M = 0 and the other for M = ±1, which is located about 8 cm^{-1} above the M = 0 level. Thus the state for M = ±1 can be studied by ESR. The ESR spectrum at X-band at 4.2°K consists of a single group of 8 lines, which are very nearly equally spaced and are separated by about 114 gauss. The spectrum is not observable at 78°K. Also, at liquid Helium II temperatures the intensities of lines are reduced, because of the depopulation of the magnetic M = ±1 state. A typical spectrum and its angular dependence are shown in Figs. 2 and 3. An interesting fact is that the hfs components are about 110 gauss apart, or about $1.02 \times 10^{-4} cm^{-1}$. This value is smaller than that for V^{4+}. Information on $g_{\perp}$ and B is still lacking.

The ESR spectrum for V^{2+} can be produced by subjecting sapphires containing vanadium to ionizing radiations. Figure 4 gives the spectrum obtained from so-called green sapphire, which contains a small amount of vanadium and cobalt. This spectrum was taken at K-band frequencies. There are three groups of 8 lines, indicating that the electron spin of the center is 3/2, and the characteristic 8-line structure shows that this spin is due to vanadium. The strong lines accompanying the vanadium lines are due to Cr^{3+}, which is isoelectronic with V^{2+}. The relative positions of the V^{2+} and Cr^{3+} lines indicate that the zero-field splitting, 2D, for V^{2+} is somewhat smaller than that

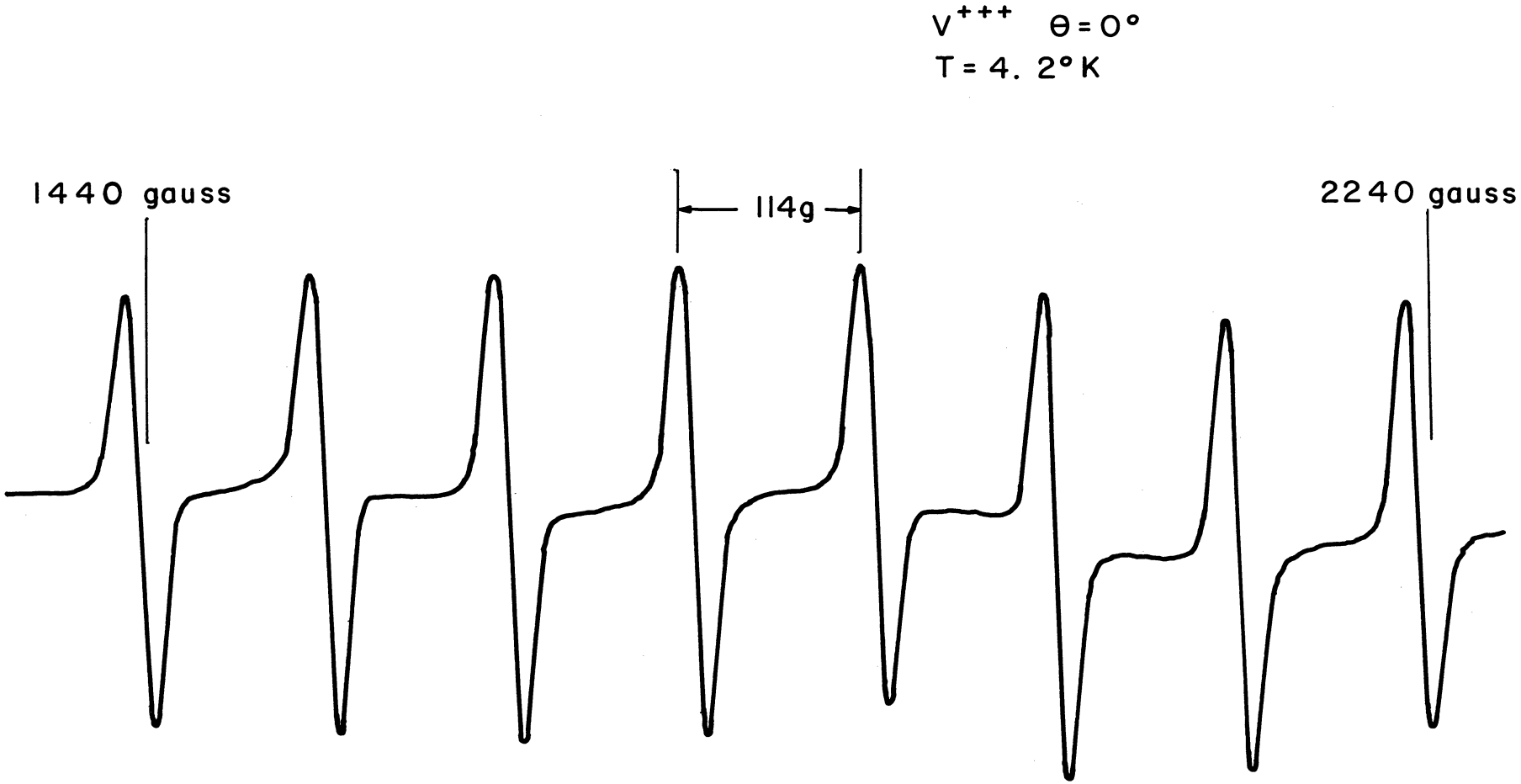

Fig. 2. ESR spectrum of V^{3+} in sapphire.

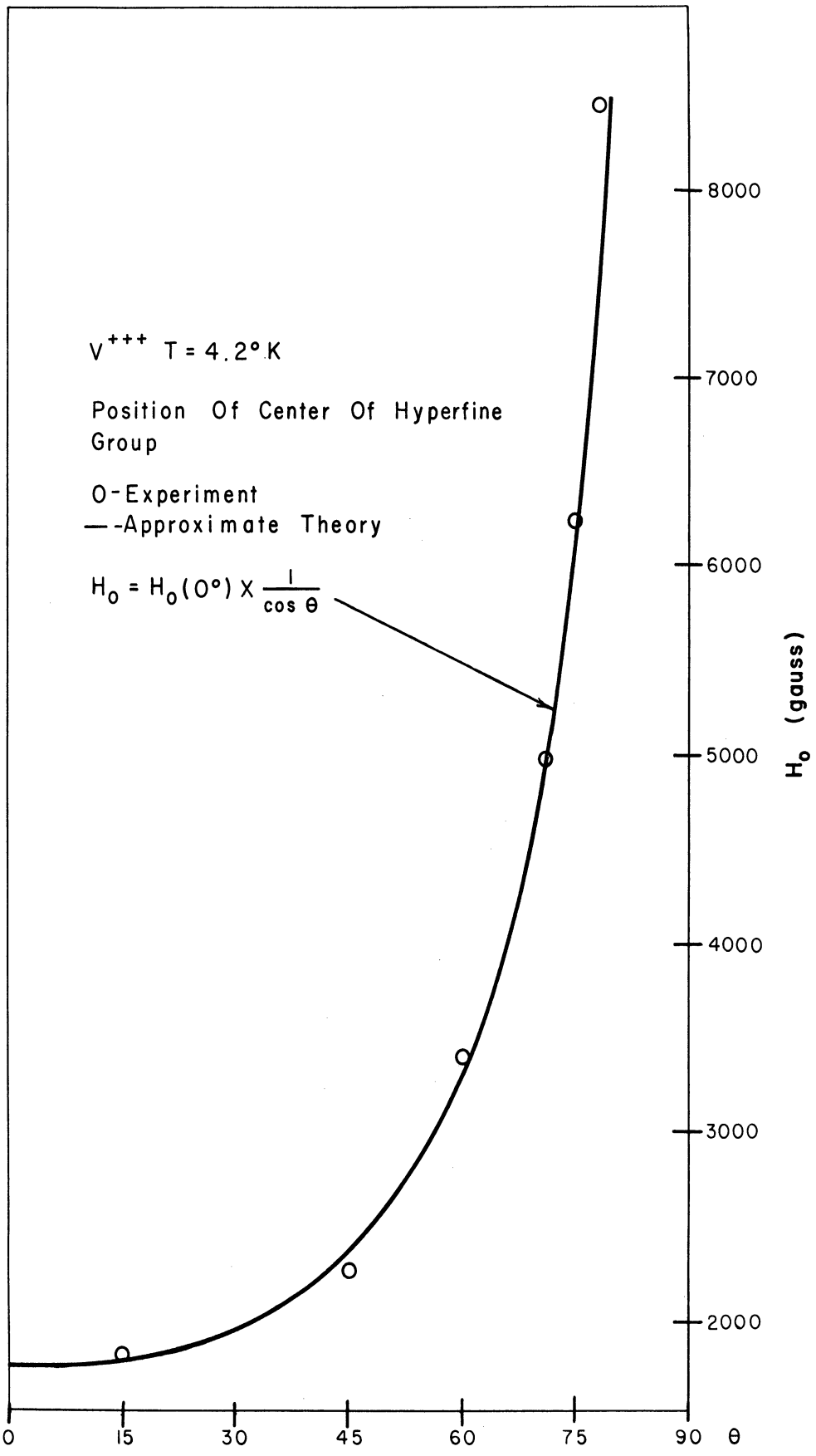

Fig. 3. Angular dependence of ESR spectrum of V^{3+} in sapphire.

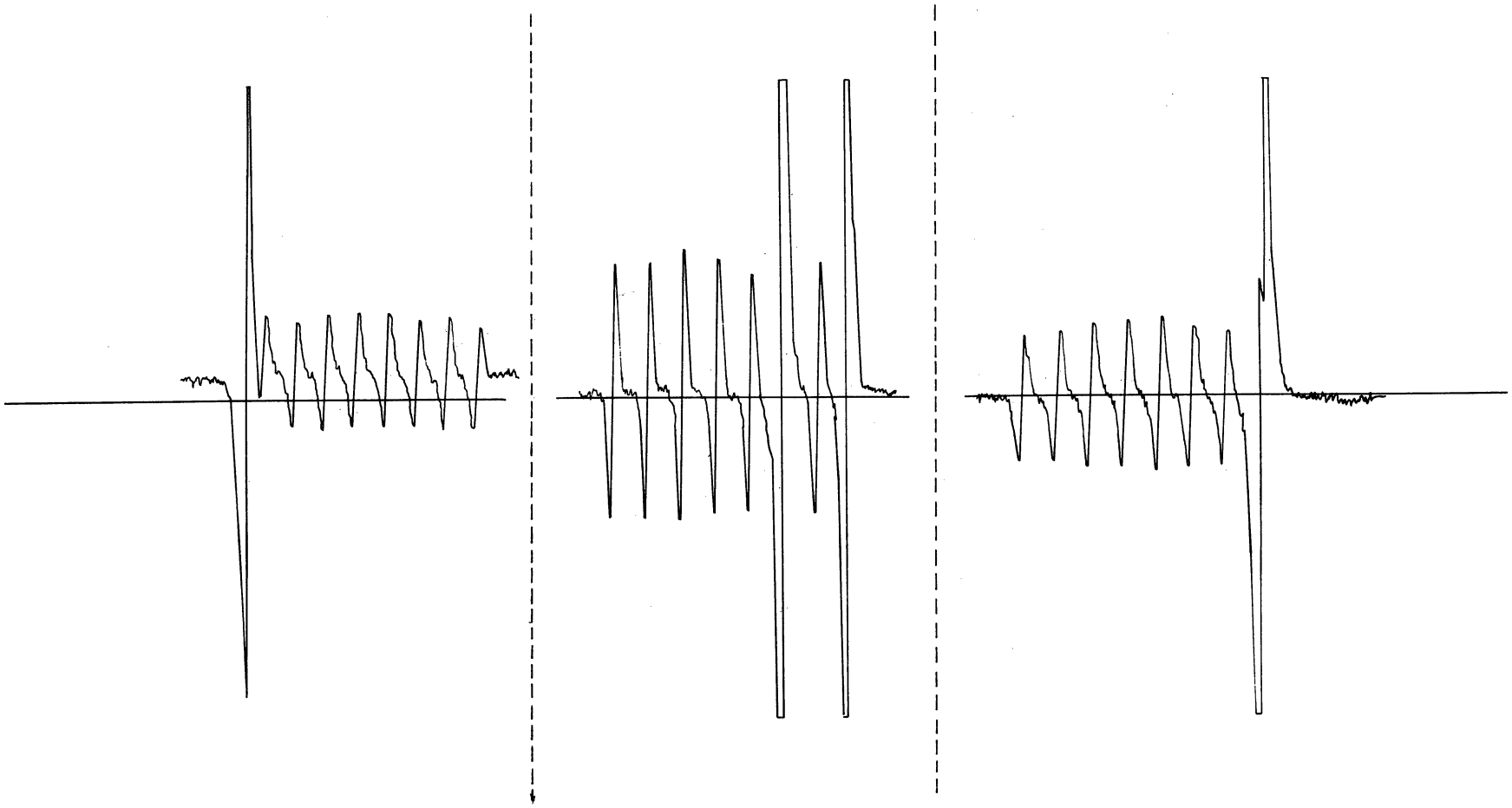

Fig. 4. ESR spectrum for V^{2+}, in green sapphire at K-band.

for Cr^{3+}. Our measurements indicate that $2D(V^{2+}) = 9.8$ kmc/sec, and is to be compared to $2D(Cr^{3+}) = 11.5$ kmc/sec. For V^{2+}, $g = 1.98$; for Cr^{3+}, $g = 1.97$.

In developing electron spin resonance, the ESR spectrometer frequency must be carefully chosen. For example, the spectrum for vanadium shown in Fig. 4 was taken at K-band frequencies. As will be noted, this spectrum consists of three groups of 8 well defined lines. Figure 5 shows the same spectrum taken at X-band frequencies. This spectrum is actually the central group of the V^{2+} spectrum, due to the transitions $M = -1/2 \rightarrow 1/2$, and is obviously very complex, the characteristic 8-line structure being absent. The high field group, however, is quite normal, as shown in Fig. 6. The complex structure of the spectrum shown in Fig. 5 can easily be explained by reference to the energy level diagram in Fig. 7. If the effects of nuclear spin are neglected, the energy levels for the four electron spin states are given by:

$$M = 3/2 \qquad E(3/2) = 3/2\ g\beta H - D$$

$$M = 1/2 \qquad E(1/2) = 1/2\ g\beta H + D$$

$$M = -1/2 \qquad E(-1/2) = -1/2\ g\beta H + D$$

$$M = -3/2 \qquad E(-3/2) = -3/2\ g\beta H - D$$

The two levels $M = 3/2$ and $M = 1/2$ cross at

$$H = 2D/g\beta$$

and furthermore the level separation of $M = -1/2$ and $M = 1/2$ is

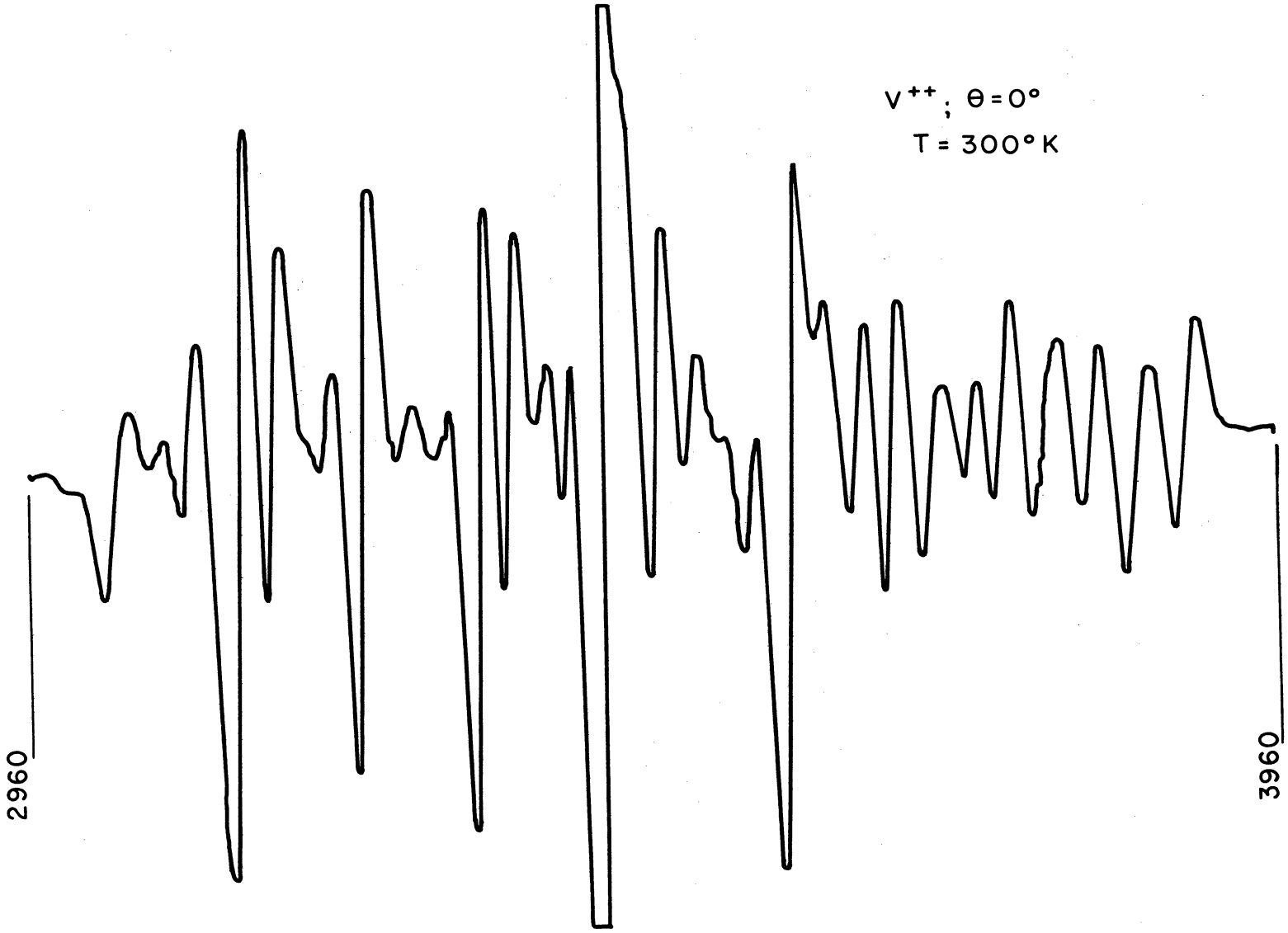

Fig. 5. ESR spectrum for V^{2+}, in green sapphire at X-band.

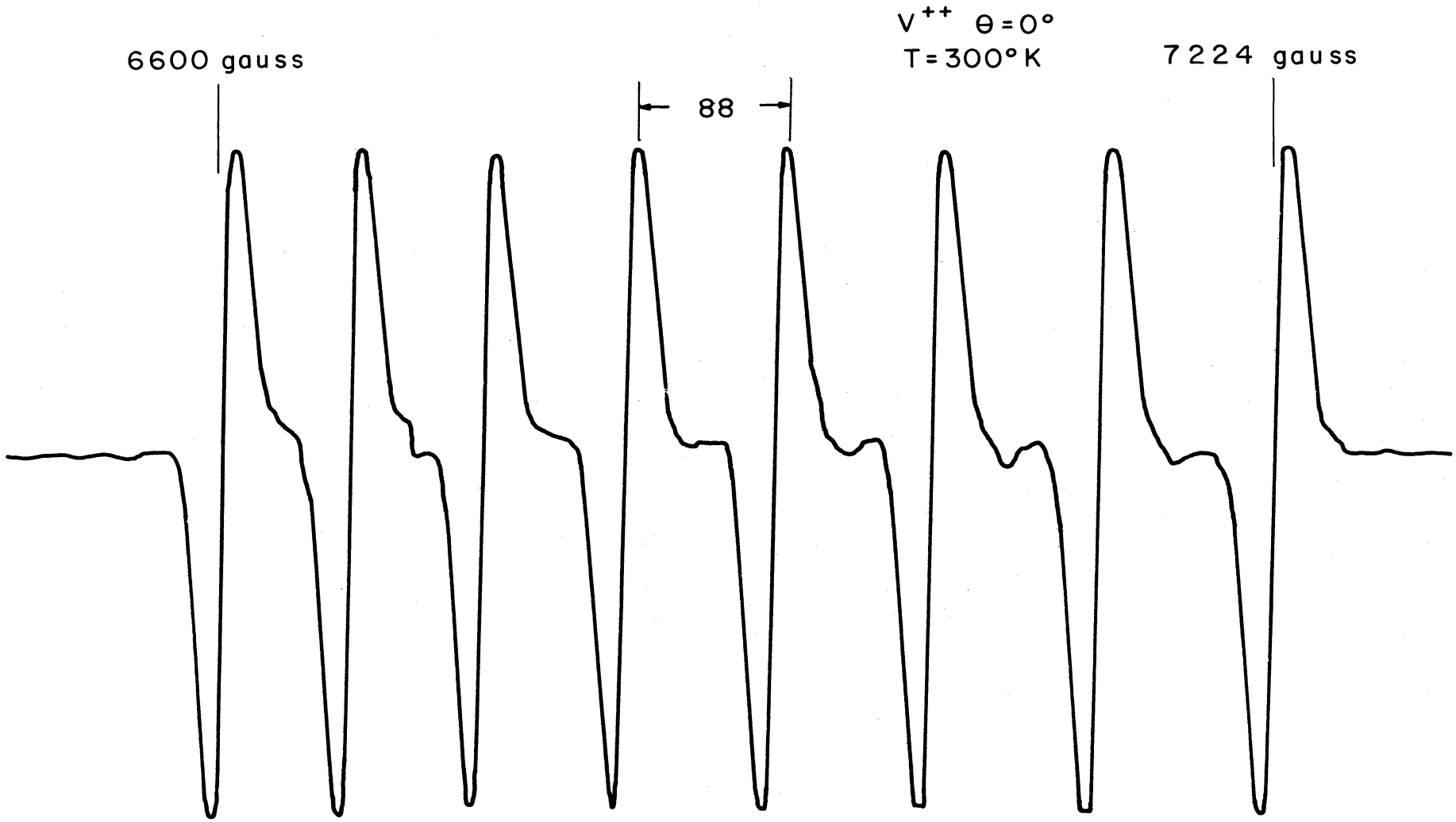

Fig. 6. High field group for V^{2+} in green sapphire at X-band.

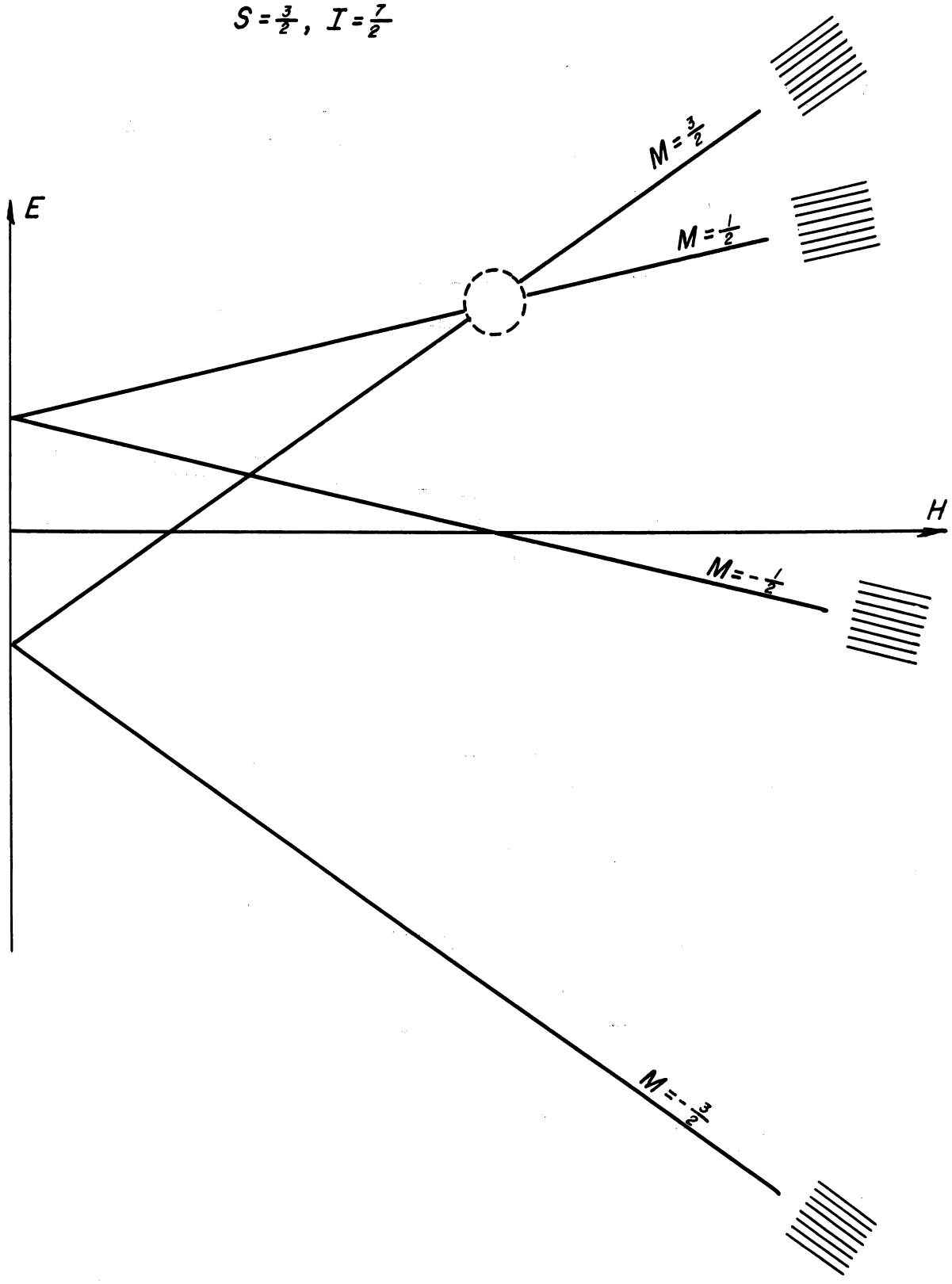

Fig. 7. Energy level diagram for V^{2+} in sapphire.

$$E(1/2) - E(-1/2) = g\beta H = 2D .$$

As pointed out earlier, 2D = 9.8 kmc/sec, which is in the X-band region. Now if the nuclear spin effect is included, the level with M = 1/2 and m will interact with the level with M = 3/2 and m-1. This results in mixing of the states, which in turn leads to a partial breakdown of the normal selection rule $\Delta M = \pm 1$, and $\Delta m = 0$. As mentioned in Section IV, it is for this reason that in the study of vandium in Al_2O_3 powder, the measurements are taken at K-band frequencies. Even at this frequency, however, it appears that we are not sufficiently far away from the cross-over point; consequently, for Al_2O_3 it would be desirable to go to even higher frequencies, possibly to the Ka-band.

Another question raised by this study is the source of the electrons responsible for the conversion of V^{3+} to V^{2+}. The electrons do not appear to come from other V^{3+} ions, because the V^{4+} signal is not affected by irradiation. Furthermore, the saturation intensity of the V^{2+} spectrum seems to vary from sample to sample, and to date the factors that determine the amount of V^{4+} have not been ascertained. The programs in oriented vanadyl radicals and vanadium in powders are being carried out to obtain information on the mechanisms responsible for the conversion of one vanadium valence state to another, and on the determination of chemical impurities and crystal defects responsible for the stabilization of particular valence states in crystals.

The practical reason motivating our investigations is that the stabilization of specific valence states is important in preparing materials for solid-

state devices. For example, V^{2+} is isoelectronic with Cr^{3+}, so that a properly prepared vanadium sapphire could be a material useful for masers and lasers, particularly in the presence of ionizing radiations.

III. ORIENTED VO^{++} IONS IN TUTTON SALTS

In order to find answers to the questions raised by our study of vanadium sapphire, we turned to vanadyl radicals in Tutton salts because these crystals can be easily grown in our laboratory, and furthermore, as our preliminary studies showed, the VO^{++} can be readily converted to V^{++} by means of X-rays. Since only a brief report of our results has been made so far,[9] some additional details will be given here.

It should be noted that randomly oriented VO^{++} has been studied by a number of investigators. Among the first to make a study of VO^{++} in frozen aqueous solution was Kozyrev.[14] Investigation of VO^{++} radicals on various adsorbers was carried out by Faber and Rogers;[15] vanadyl porphyrins by Roberts, Koski and Caughey;[16] vanadyl etioporphyrins dissolved in benzene and high viscosity oil by O'Reilly;[17] and vanadyl ions in aqueous, solutions by Pake and Sands,[18] and Sands.[19] Much of the interest in the vanadyl ion appears to have been stimulated by oil companies which were concerned with the relatively high concentration of vanadyl vanadium in crude oil and its effect on the technology of refinery operation. Because the presence of vanadium in oil also casts some light on the nature of organisms involved in the production of petroleum, some geologic interest has been stimulated as well.[20]

Despite this relative wealth of studies of randomly oriented VO^{++} in solutions, very few studies of oriented VO^{++} have appeared. Brief comments on tetravalent vanadium occur in the paper by Hutchison and Singer,[21] and some unpublished investigations by W. B. Gager[22] exist. Consequently we have

undertaken a systematic study of VO^{++} radicals in the Tutton salts to determine whether vanadium occurs as VO^{++} or V^{4+} in these crystals, and to study the relation of V^{++} produced by ionizing radiation to that grown directly intc the crystal. Our studies reveal that VO^{++} maintains its identity in these crystals, and that, following irradiation, the vanadyl vanadium is converted to V^{++} which is indistinguishable from that grown directly into the crystal lattice. These conclusions are based on the fact that the vanadous vanadium, V^{2+}, produced by irradiation from VO^{++} in the Tutton salt, has within experimental error the same spin-Hamiltonian parameters and the same orientation of crystalline electric field as those of V^{++} Tutton salt grown from aqueous solution. While our investigations were in progress, the paper by Ballhausen and Gray[23] appeared. We feel that the validity of their theoretical calculations is confirmed by our experimental results.

The crystal structure of the Tutton salts is quite complex. There are two non-equivalent sites, and about each divalent metal ion site—in which VO^{++} and V^{++} occur substitutionally—there are six water molecules of hydration, forming a distorted octahedron. Consider the simplified model shown in Fig. 8. The water ligands are located at the face centers of a cube, with

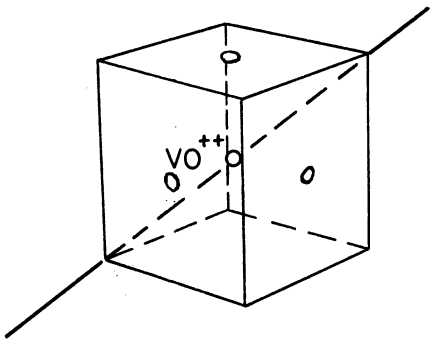

Fig. 8. Simplified model of VO^{2+} in octahedral complex.

the VO^{++} and V^{++} ions at the center. The VO^{++} radicals at the center of cube, according to our experimental results, seem to prefer directions along the body diagonal. A possible explanation for this orientation is that according to the molecular orbital calculations by Ballhausen and Gray,[23] the vanadium and oxygen in the vanadyl radical carry unequal charges, so that body-diagonal directions represent the directions of least energy. If the model suggested here were correct, the VO^{++} radical could be along any one of the four body diagonals, with equal probability. In actuality, however, the cube is badly distorted, so that certain directions become preferred. In the zinc ammonium Tutton three of the four orientations have been observed, but the populations are in the ratio of 40:10:2. The fourth direction evidently has a population too low to be detected by ESR.

A partial summary of our results is presented in Table I.

TABLE I

EXPERIMENTAL RESULTS FOR VO^{2+}

	Orientation 1	Orientation 2	Powder	Calculated[23]
$g_{\|\|}$ =	1.9328±2	1.9314±2	1.935	1.940
$g_{\perp}$ =	1.9802±3	1.9812±3	1.98	1.983
$\langle g \rangle$ =	1.9644±3	1.9646±2	1.965	1.969
$\|A\|$ =	0.01824±2/cm		0.0182/cm	---
$\|B\|$ =	0.007162±5/cm		0.0729/cm	---

Several interesting facts stand out. One is that for the two orientations, the individual g-values differ appreciably. Yet the average g-values are equal, within experimental error. This perhaps is to be expected if the crystalline field provides the major contribution to Δg. For the two sites, the crystalline fields have different orientations with respect to the VO^{++}, but the trace of the g-tensor should be the same if the ligand bonding effects do not change.

Another interesting fact is the excellent agreement of the single crystal and powder measurements. Thus, for the VO^{++} radical, sufficiently reliable results can be obtained from powder measurements provided the resonances are not broadened by the inhomogeneous "crystal" field. In Fig. 9 we show the spectrum of VO^{++} in crushed zinc ammonium Tutton salt, which is to be compared to the spectra of VO^{++} absorbed on Amberlite IR-4B and of vanadium in glass shown in the same figure. The last spectrum indicates that vanadium is present as vanadyl vanadium in glass. The powder measurements can be explained from the single crystal measurements as shown in Fig. 10.

The remarkably good agreement between theory and experiment should perhaps be noted. We need, however, to be somewhat cautious in applying these theoretical results, because the calculations by Ballhausen and Gray apply to $[VO(H_2O)_5]^{2+}$ where there are only five water ligands in tetragonal symmetry. Therefore the model given in Fig. 11 was used. The distance to the water ligands was taken to be 2.3A and that to the vanadyl oxygen 1.67A. Molecular orbital calculations indicate the charge distribution $V^{+0.97}O^{-0.60}(5H_2O)^{+1.63}$. We are planning to make corresponding calculations with an

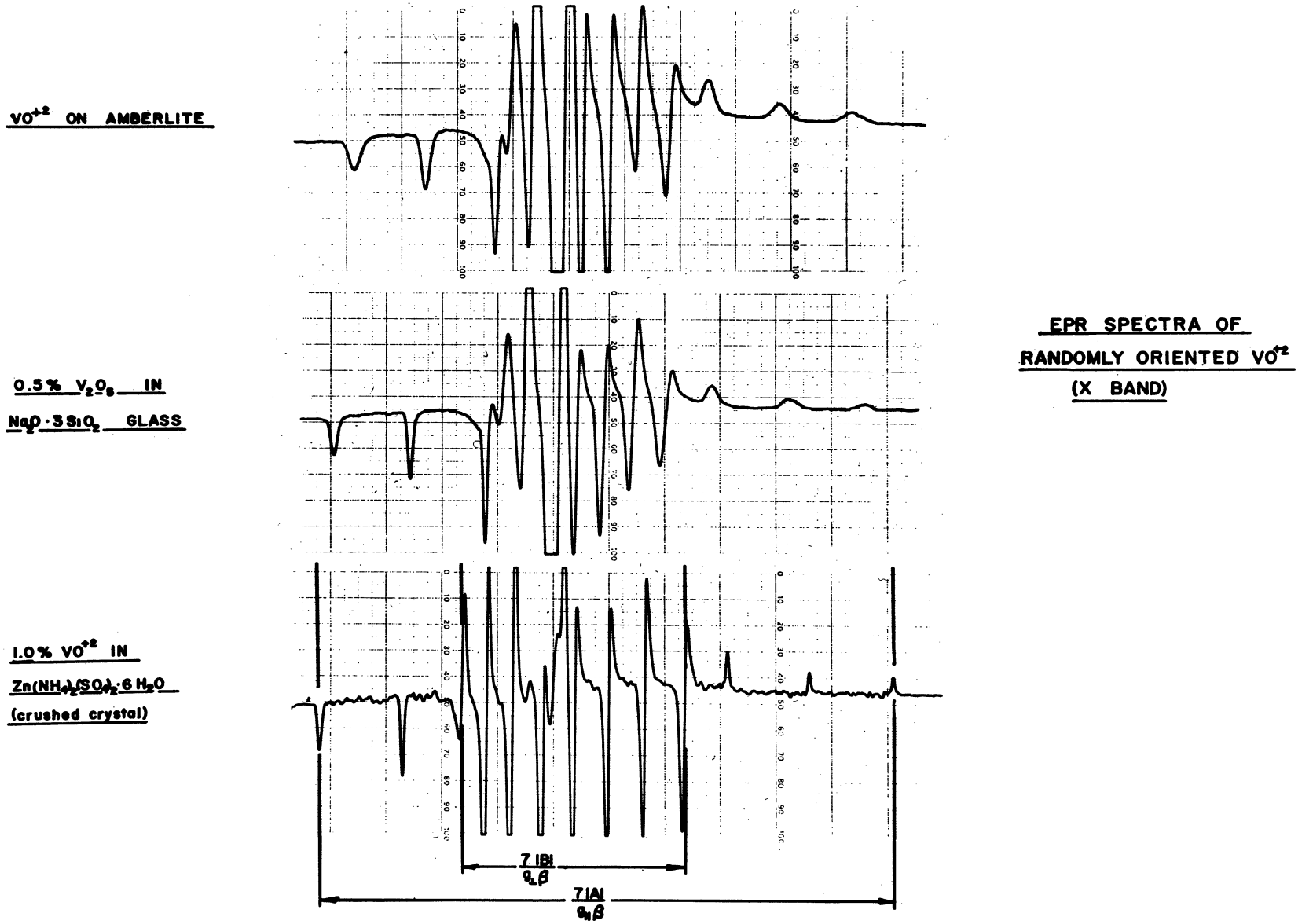

Fig. 9. EPR spectra of randomly oriented VO^{+2} (X-band).

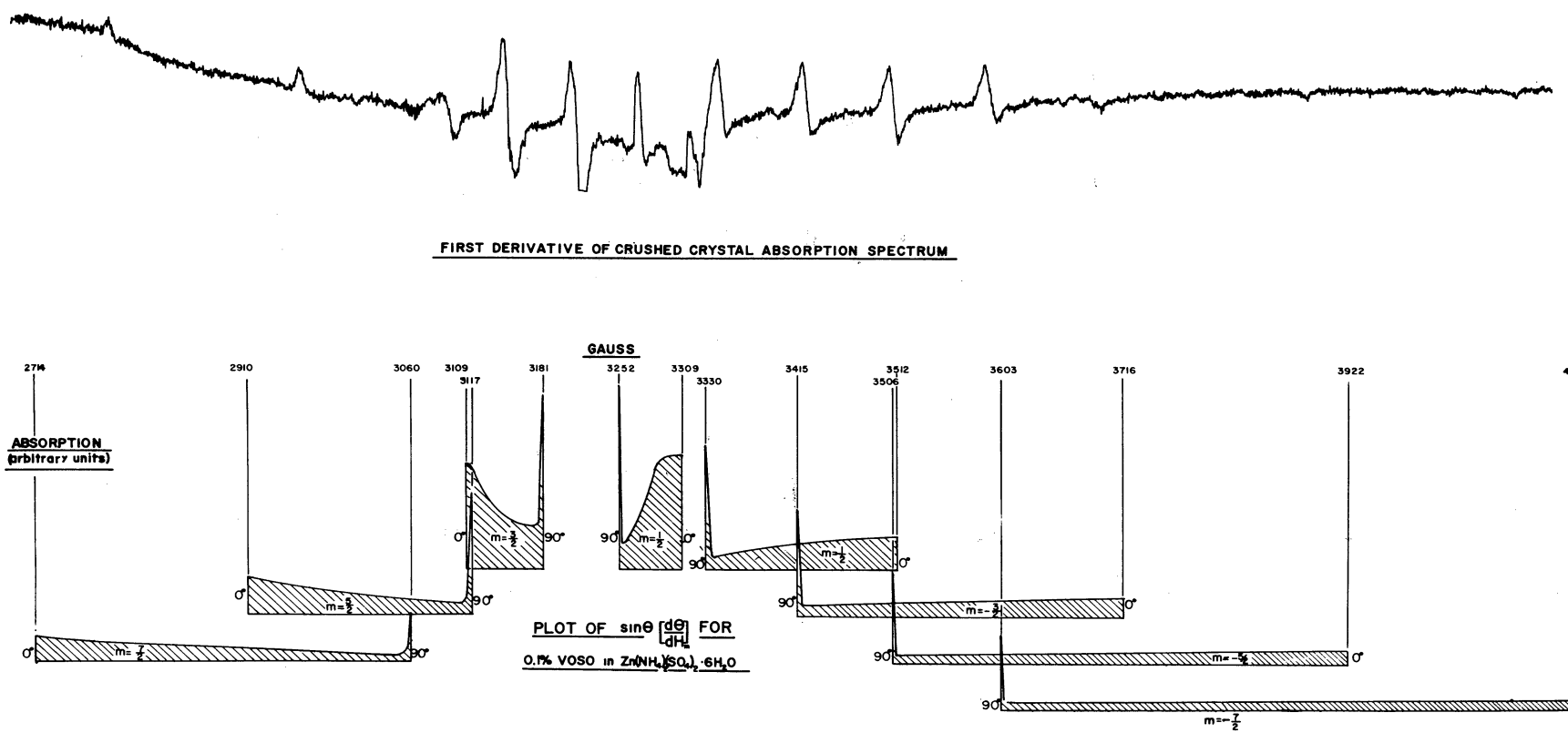

Fig. 10. Plot of sin θ $[d\theta/dH]_M$ for 0.1% $VOSO_4$ in $Zn(NH_4)_2(SO_4)_2 \cdot 6H_2O$.

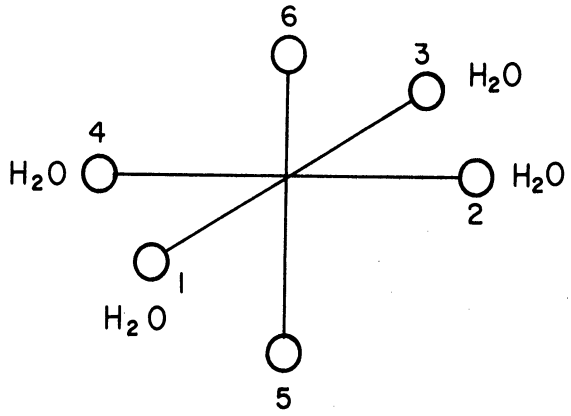

Fig. 11. $[VO(H_2O)_5]^{2+}$.

octahedral arrangement of the water ligands and the VO^{++} axis along the body diagonal.

Although we must wait for the results of these molecular orbital calculations, we can nevertheless make a few qualitative comments on the relation of the g-values to the optical absorption spectrum. If we assume that the vanadyl oxygen provides a large field of cylindrical symmetry, and that the ligand waters provide an additional field of trigonal symmetry with small rhombic component, the energy level diagram will be as indicated in Fig. 12.

If the orbital levels are at Δ and Δ' respectively above the ground state, and if the spin-orbit coupling parameter is small in comparison to these orbital splittings, then perturbation calculation shows that

$$g_{\parallel} = 2\left(1 - \frac{4\lambda}{\Delta'}\right)$$

$$g_{\perp} = 2\left(1 - \frac{\lambda}{\Delta}\right)$$

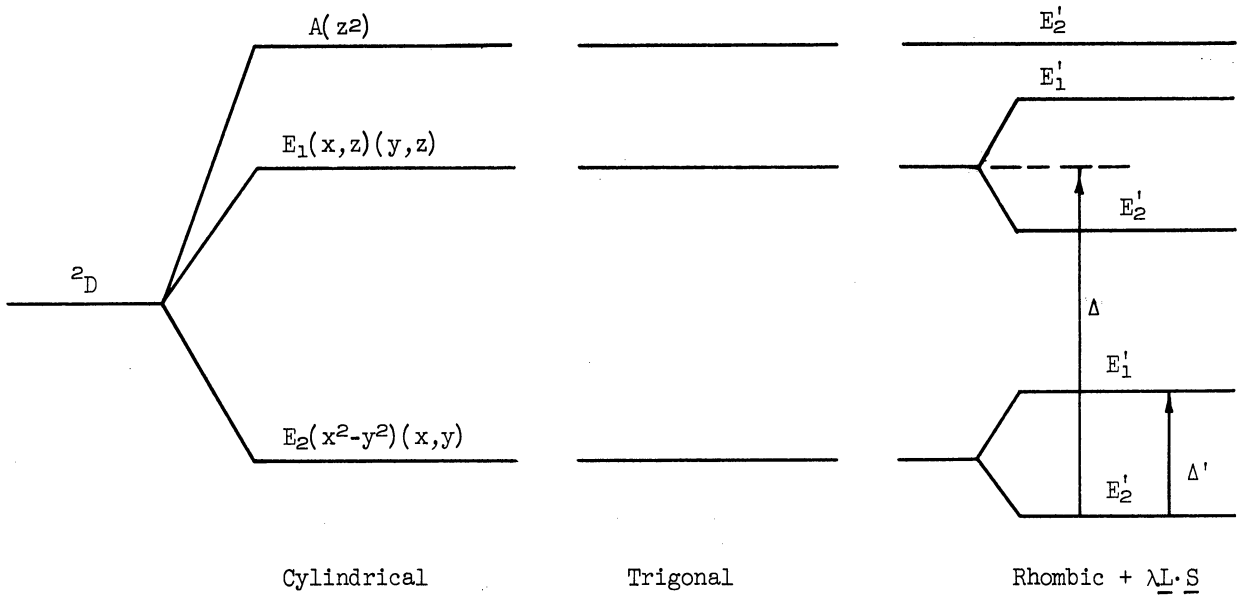

Fig. 12. Energy level diagram for VO^{2+} in octahedral complex.

Using

$$g_{\parallel} = 1.9328, \qquad g_{\perp} = 1.9802$$

for the zinc ammonium Tutton salt, we find that

$$\Delta'/\Delta = \frac{(\lambda/\Delta)}{(\lambda/\Delta')} = .0099/.0084 = 1.2$$

Optical measurements on Tutton salts have not yet been made, but it is anticipated that the absorption spectrum will not be too dissimilar from that of $VO_2O_4\ 5H_2O$ in aqueous solution. Measurements indicate the presence of

crystal field bands at 13,000 cm^{-1} and 16,000 cm^{-1} respectively. If these are identified with Δ and Δ' we obtain

$$\Delta'/\Delta = 16{,}000/13{,}000 = 1.2$$

which is in good agreement with the results from g-value measurements.

Furthermore, it should be noticed that in the VO^{++} discussed so far, $g_\perp$ is invariably larger than $g_{||}$. This is taken as evidence that the vanadium is strongly bonded to the oxygen and is not present as isolated V^{4+}. The g-values for VO^{++} are in considerable contrast to those for vanadium in rutile as reported by Gerritsen and Lewis.[24] They report $g_\perp = 1.914$ and $g_{||} = 1.956$. This marked difference, in which $g_\perp$ is less than $g_{||}$, is perhaps to be expected because the crystal structure suggests that the vanadium is not preferentially bonded to one oxygen. If the vanadium does not distort the lattice, there would be four planar oxygens at the corners of a rectangle at 1.88A and two oxygens on the vertical axis at 1.97A. These oxygens are shown in Fig. 13.

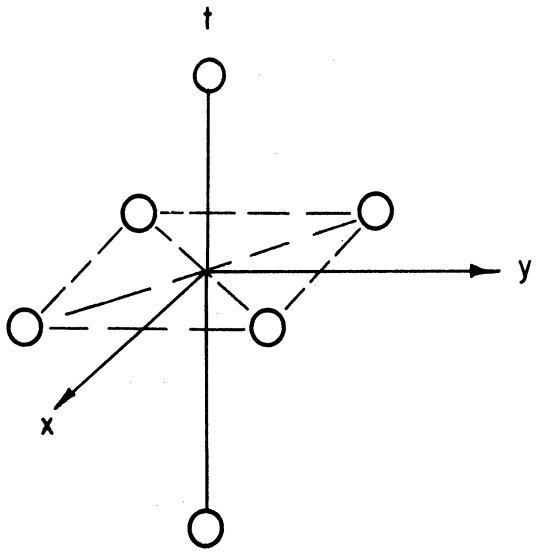

Fig. 13. V^{4+} in rutile.

As indicated earlier, the irradiation of these crystals by ionizing radiation leads to the conversion of VO^{++} to V^{++}. A comparison of the spectrum before and after irradiation is given in Table II. The bottom spectrum is that of irradiated zinc ammonium Tutton salt containing V^{++}. The spin-Hamiltonian parameters are listed below.

TABLE II

EXPERIMENTAL RESULTS FOR V^{++}

	V^{++}(Irradiated VO^{++})	V^{++}(Grown)	V^{++}(Ref. 6)
$g_{\parallel}$ =	1.9719±3	1.9718±3	1.951±2
$g_{\perp}$ =	1.9745±5	1.9750±5	---
|D| =	0.15609±3/cm	0.15611±3/cm	0.158±10/cm
|E| =	0.02303±3/cm	0.02297±3/cm	0.049±50/cm
|A| = |B| =	0.008270±5/cm	0.008270±5/cm	0.0088±2/cm

It is concluded from these results that the two vanadous vanadiums incorporated directly into the lattice obtained by converting VO^{++} are not distinguishable. This suggests that the effect of radiation is to remove oxygen to a distance where its presence becomes negligible in affecting the spin resonance properties of V^{++}. Figure 14 gives these spectra for VO^{++}, irradiated VO^{++}, and unirradiated V^{++} in zinc ammonium Tutton salt.

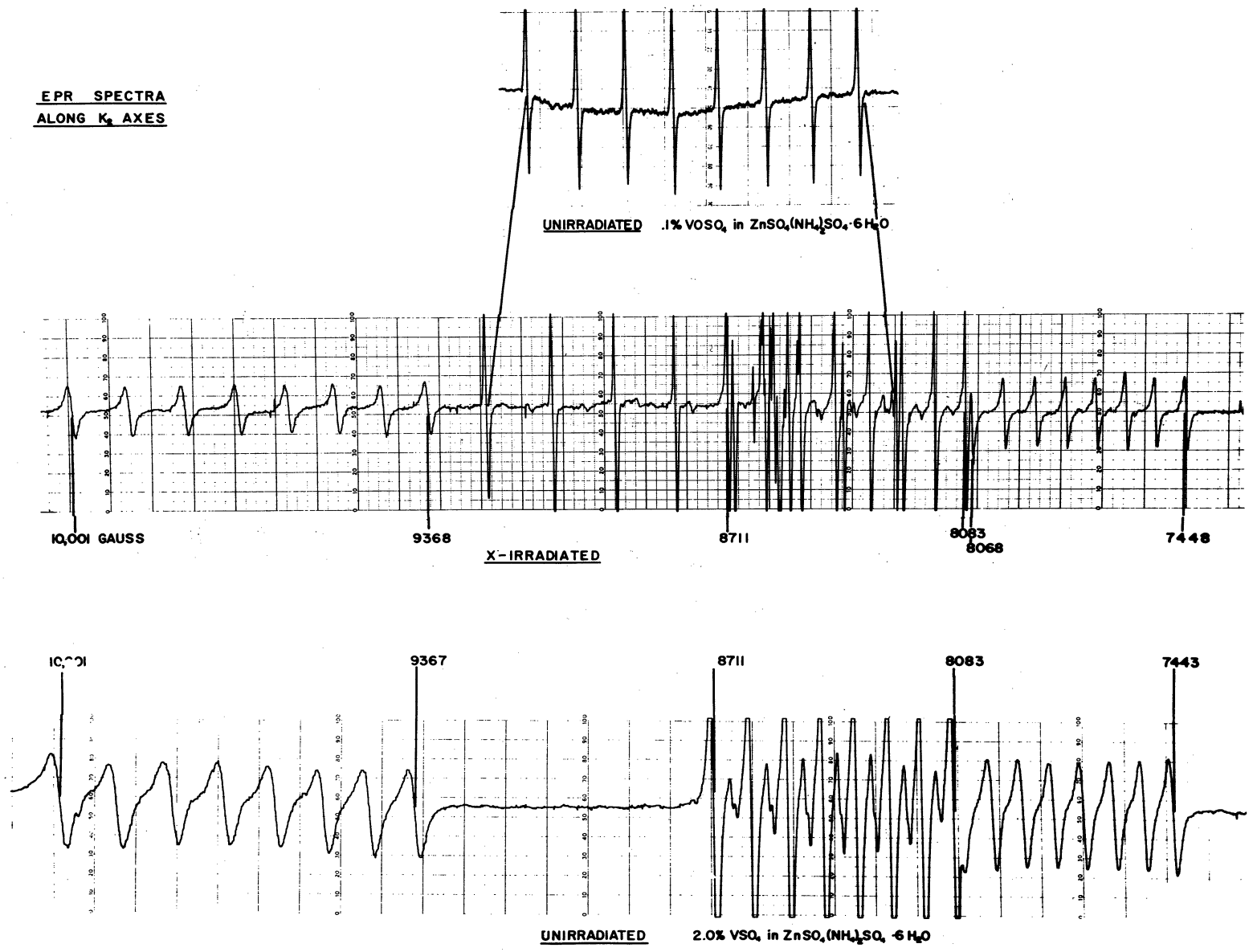

Fig. 14. VO^{2+} and V^{2+} in zinc ammonium sulfate.

IV. VANADIUM IN POWDERS

As noted earlier, in our studies of vanadium sapphire we were unable to ascertain sources for the electrons responsible for the conversion of V^{3+} to V^{2+} under irradiation. Consequently, we thought it might be more appropriate to study first the properties of vanadium in easily prepared powders, and then, when the recipe was worked out, to go to single crystals. As mentioned earlier, one reason for our interest in powders was to complement the known information on other isoelectronic ions such as Cr^{3+} and Mn^{4+}. Another reason for our interest is that we hope to use some of these techniques to measure nuclear spins and magnetic moments. The nuclide of particular interest to us is V^{49}. The nuclear spin and magnetic moment of this nuclide, which under electron capture transforms to Ti^{49} with 330-day half-life, were first reported by Weiss, Walter, Gilliam, and Cohen.[25] However, the observations were in a xylene solution of a vanadium (IV)-cupferron chelate, where the individual vanadium hfs lines are quite broad. Therefore the very weak V^{49} signals were almost obscured by the occurrence of strong V^{51} lines as an impurity. Preliminary estimates show that if V^{49} can be incorporated into MgO powder, the hfs lines are very sharp, so that a fairly high precision value for the nuclear magnetic moment can be obtained.

Consequently, we shall present some of the preliminary results of our work on MgO and Al_2O_3 powders, despite the fact that our investigations are far from being complete.

The MgO powder samples containing vanadium are prepared by wetting MgO powder with a solution of $VOSO_4$, so as to obtain about 0.1% for the V/Mg ratio. The samples are then dried, fired at a suitable temperature, and irradiated with 50 Kev X-rays. The dried samples often exhibit a spectrum suggestive of VO^{++}, but this disappears completely upon firing at 900°C or higher. If, however, the sample is subsequently irradiated with X-rays, a spectrum is observed suggesting that vanadium is present as V^{2+} and/or V^{4+}.

A typical spectrum obtained from a sample heated at temperatures of about 1200°C and then X-rayed is shown in Fig. 15. There are the characteristic 8 lines corresponding to I = 7/2 for the nuclear spin of V^{51}. In addition, the principal hfs lines are flanked by two satellites, suggesting that the electron spin of the paramagnetic center is 3/2. In fact, very good agreement between theory and experiment is obtained by assuming that the satellite splitting is due to second-order effects in the electron-nuclear interaction term. Thus there is every reason to believe that the spectrum presented here is due to vanadous vanadium, V^{2+}.

If, however, the sample is fired at a lower temperature, say around 900°C, the satellites do not show up (see the lower half of Fig. 15). The absence of structure suggests strongly that the spectrum is due to a center with S = 1/2; thus its assignment to V^{4+} is suggested. But if such assignment is correct, it is hard to understand why the ESR spectrums of both V^{2+} and V^{4+} should have exactly the same g-value and hyperfine coupling constant.

We have also started a program to study vanadium in Al_2O_3 powder. For this program, as noted earlier, the powder measurements should be carried out

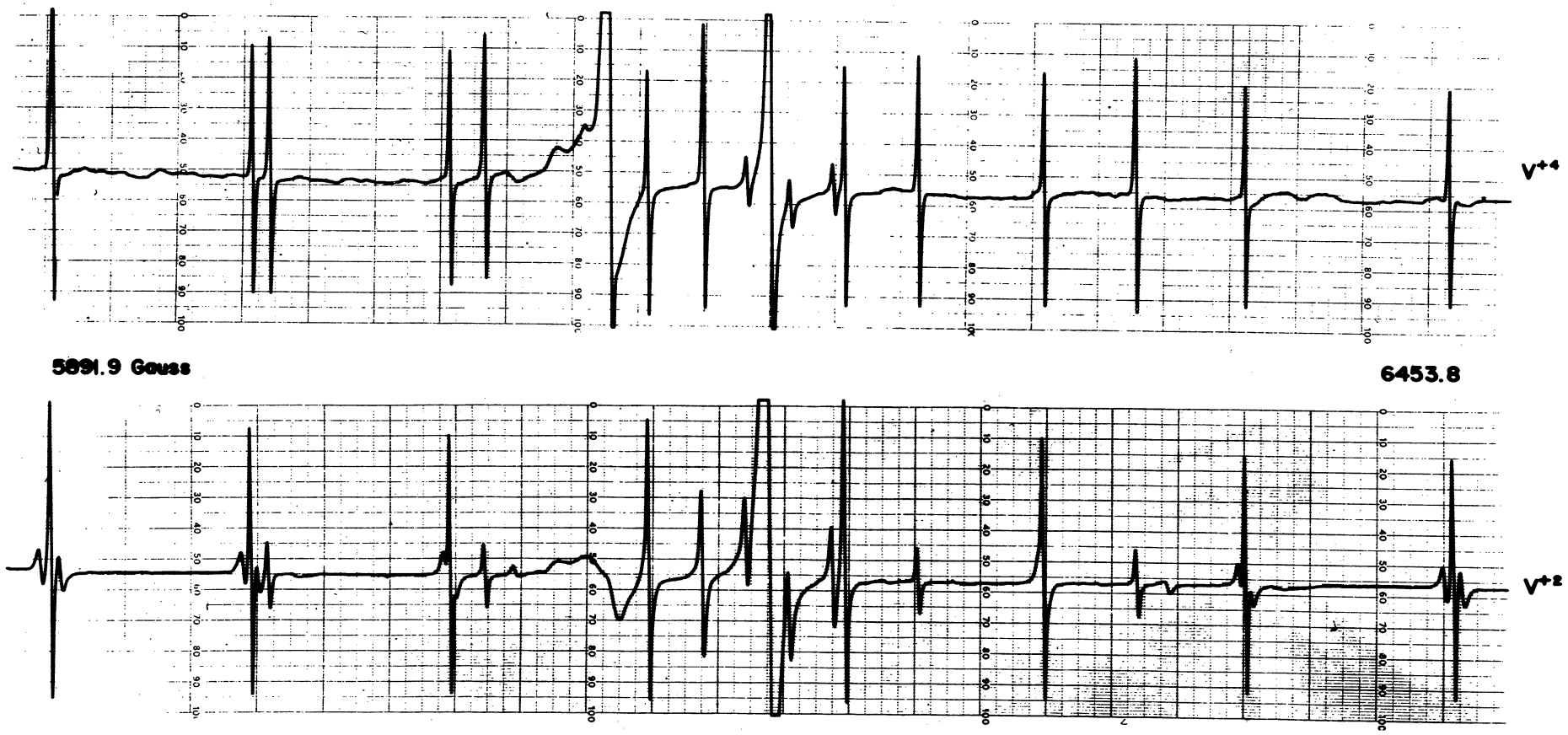

VANADIUM IN MgO POWDER

Fig. 15. Vanadium in MgO powder.

at K-band frequencies or higher. The results obtained so far indicate that vanadium can be detected in Al_2O_3 powder, but before this detection can be made the samples must be irradiated in CO_2 atmosphere. These results are preliminary, and during the next few months we hope to find more information on factors that contribute to the stabilization of vanadous vanadium.

Just recently it has been observed in our laboratory that vanadium in CaO shows a rather unexpected angular dependence quite similar to that of Mn (see Fig. 16). Thus the problem of vanadium solid-state chemistry appears to be an intriguing one, and we are confident that electron spin resonance can be developed into a useful analytical tool for the study of the valence states of vanadium.

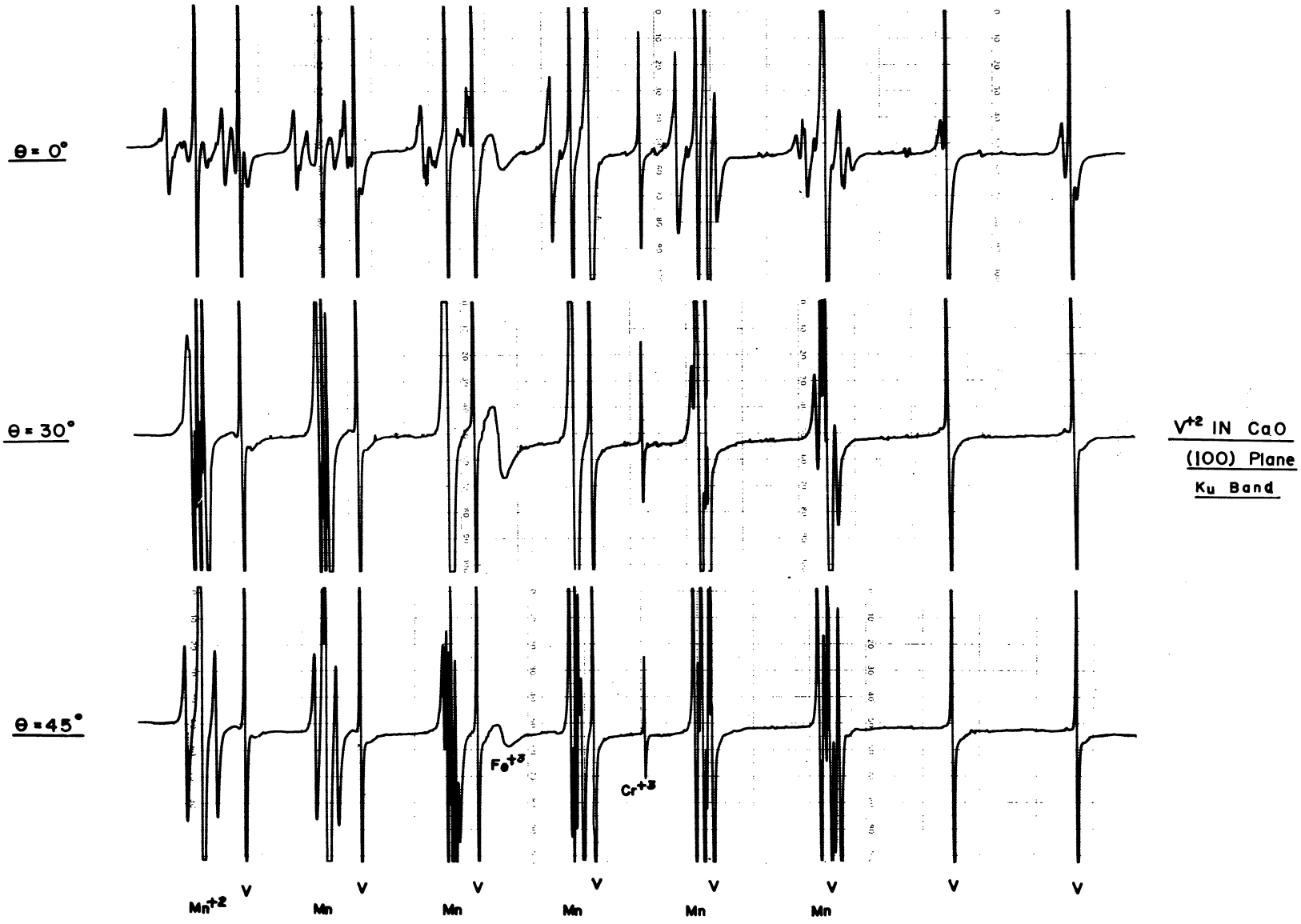

Fig. 16. V^{2+} in CaO.

V. REFERENCES

1. See for example C. Kikuchi, J. Lambe, G. Makhov, and R. W. Terhune, "Ruby as a Maser Material," J. App. Phys. 30, 1061 (1959).

2. See for example C. Kikuchi, M. H. Sirvetz, and V. W. Cohen, "Paramagnetic Resonance Hyperfine Structure of V^{50} and V^{51}," Phys. Rev. 92, 109 (1953).

3. See for example R. W. Terhune, J. Lambe, C. Kikuchi, and J. Boher, "Hyperfine Spectrum of Chromium 53 in Al_2O_3," Phys. Rev. 123, 1265 (1961).

4. See for example C. Kikuchi and V. W. Cohen, "Paramagnetic Resonance Absorption of Carbazyl and Hydrazyl," Phys. Rev. 93, 394 (1954).

5. See for example L. M. Matarrese and C. Kikuchi, "Paramagnetic Resonance Absorption of Mn^{++} in Single Crystals of Zinc Blende," J. Phys. Chem. Solids 1, 117 (1956).

6. See for example C. Kikuchi and L. M. Matarrese, "Paramagnetic Resonance Absorption of Ions with Spin 5/2: Mn^{++} in Calcite," J. Chem. Phys. 33, 601 (1960).

7. See for example C. Kikuchi and G. H. Azarbayejani, "Spin Resonance Properties of ZnTe:Mn and of Other $A_{II}B_{VI}$ Compounds," J. Phys. Soc. Japan 17, Suppl. B-1, 453 (1962).

8. J. Lambe and C. Kikuchi, "Spin Resonance of V^{2+}, V^{3+}, and V^{4+} in α-Al_2O_3," Phys. Rev. 118, 71 (1960).

9. R. Borcherts, G. Wepfer, and C. Kikuchi, "Paramagnetic Resonance Spectrum of Vanadyl Ammonium Sulfate," Bull. Am. Phys. Soc. 7, 118 (1962).

10. G. M. Zverev and A. M. Prokhorov, "Electron Paramagnetic Resonance of the V^{+++} Ion in Sapphire," Soc. Phys. JETP 7, 1023 (1958).

11. A. Siegert, "Zur Dentung des magnetischen Verhaltens der Alaune der Eisengruppe," Physica 4, 138 (1937).

12. J. van der Handel and A. Siegert, "Über das magnetischen Verhalten vom Vanadium - Ammonium Alaum," Physica 4, 871 (1937).

13. M. H. L. Pryce and W. A. Runciman, "The Absorption Spectrum of Vanadium Corundum," Disc. Faraday Soc. 26, 34 (1958).

14. B. M. Kozyrev, "Paramagnetic Resonance in Solutions of Electrolytes," Disc. Faraday Soc. 19, 135 (1955).

15. R. J. Faber and M. T. Rogers, "Paramagnetic Resonance Spectra of Absorbed Manganese (II), Copper (II) and Oxovanadium (IV)," J. Am. Chem. Soc. 81, 1849 (1959).

16. C. M. Roberts, W. S. Koski, and W. S. Caughey, "Electron Spin Resonance of Some Vanadyl Porphyrins," J. Chem. Phys. 34, 591 (1961).

17. D. E. O'Reilly, "Paramagnetic Resonance of Vanadyl Etioporphyrin I," J. Chem. Phys. 29, 1188 (1958).

18. G. E. Pake and R. H. Sands, "Hyperfine Structure in the Paramagnetic Resonance of Vanadium Ions in Solution," Phys. Rev. 98, 266A (1955).

19. R. H. Sands, "Paramagnetic Resonance Absorption in Glass," Phys. Rev. 99, 1222 (1955).

20. A. J. Saraceno, D. T. Fanale, and N. D. Coggeshall, "An Electron Paramagnetic Resonance Investigation of Vanadium in Petroleum Oils," Analytical Chem. 33, 500 (1961).

21. C. A. Hutchinson and L. S. Singer, "Paramagnetic Resonance Absorption in Salts of V and Mn," Phys. Rev. 89, 256 (1953).

22. In a private communication, Dr. W. B. Gager of the Battelle Memorial Institute has informed us that he too has made some preliminary unpublished investigations of VO^{++} in Tutton salts. However, a complete identification of the centers was not made.

23. C. J. Ballhausen and H. B. Gray, "The Electronic Structure of the Vanadyl Ion," Inorganic Chemistry 1, 111 (1962).

24. H. J. Gerritsen and H. R. Lewis, "Paramagnetic Resonance of V^{4+} in TiO_2," Phys. Rev. 119, 1010 (1960).

25. M. M. Weiss, R. I. Walter, O. R. Gilliam, and V. W. Cohen, "Paramagnetic Resonance Spectrum of V^{49}," Bull. Am. Phys. Soc. 2, 31 (1957).

PART B

MOLECULAR ORBITAL (MO) TREATMENT OF VANADYL COMPLEX ION

by

Inan Chen

I. INTRODUCTION

The evidence of electron delocalization in transition element complex, such as super-hyperfine structure and reduction of spin-orbit coupling constant,[1-3] suggests the use of molecular orbital (MO) treatments. The MO treatment has been widely used by chemists for the claculation of organic molecules and inorganic diatomic molecules.[4-7] Wolfsberg and Helmholz[8] were the first to use this method for inorganic complex ions. In the following, we will discuss the MO treatment of vanadyl complex by Ballhausen and Gray.[9]

II. CRYSTAL FIELD THEORY OF VO^{++} COMPLEX

Since the environment of V^{4+} in vanadyl complex is a distorted octahedron as shown in Fig. 1, we can consider the crystal field as the sum of a cubic field which belongs to O_h and a tetragonal field which belongs to C_{4v}. From group theory we know that in cubic field, 3d level will split into two levels, e_g and t_{2g}. These two levels will split again in tetragonal field into

$$e_g \longrightarrow a_1 + b_1$$

$$t_{2g} \longrightarrow e + b_2$$

as shown in Fig. 2. The d orbitals belonging to these levels and their energies are also shown in Fig. 2. These energies are obtained by calculating

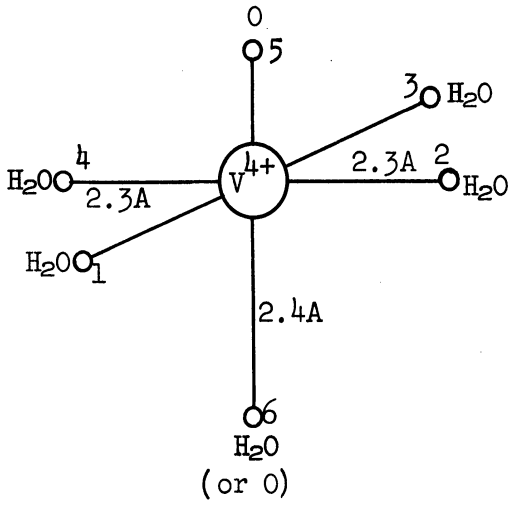

Fig. 1. Structure of VO^{++} complex ion. The four water molecules in xy plane are equivalent; the 5th ligand is the vanadyl oxygen; the 6th ligand is a water molecule in the case of aqueous solution and is a oxygen atom in the case of crystal.

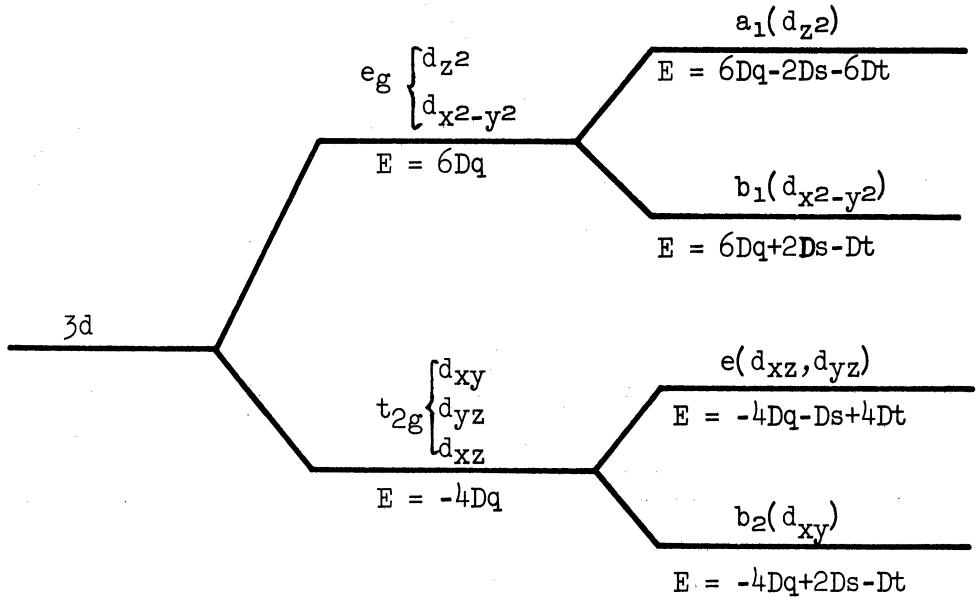

Fig. 2. Energy levels of vanadyl complex in crystal field of O_h and compressed C_{4v} symmetry.

the diagonal matrix elements of the crystal field as follows:

$$V_{c.f.} = V_{cubic} + V_{tetragonal}$$

$$= A'_{4o} r^4 \left[Y_{4o} + \left(\frac{5}{14}\right)^{1/2} (Y_{44}+Y_{4\bar{4}}) \right] + \left[A_{2o} r^2 Y_{2o} + A''_{4o} r^4 Y_{4o} \right]$$

Dq, Ds, and Dt are related to the coefficients A'_{4o}, A_{2o}, and A''_{4o} as follows:

$$Dq = \frac{1}{14\sqrt{\pi}} A'_{4o} \overline{r^4}$$

$$Ds = \frac{-\sqrt{5}}{14\sqrt{\pi}} A_{2o} \overline{r^2}$$

$$Dt = -\frac{1}{14\sqrt{\pi}} A''_{4o} \overline{r^4}$$

From the energy level diagram in Fig. 2 we can expect the electron transition shown in Table I.

TABLE I

ELECTRON TRANSITIONS

Transition	Energy Difference	Observed Wave Number
$b_2 \rightarrow e$	$-3Ds + 5Dt$	13,000 cm^{-1}
$b_2 \rightarrow b_1$	$10Dq$	16,000
$b_2 \rightarrow a_1$	$10Dq-4Ds-5Dt$	30,000 (covered by charge transfer spectrum)

The value of Dq obtained here ($Dq = 1600\ cm^{-1}$) is considerably smaller than the value of 2600 cm^{-1} which might be expected for V^{4+} by extrapolating the Dq for $V(H_2O)_6^{++}$(1220 cm^{-1}) and for $V(H_2O)_6^{+++}$(1900 cm^{-1}).

The values of Ds and Dt can be calculated by making the reasonable assumption that the third transition ($b_2 \rightarrow a_1$) occurs at 35,000 cm^{-1}. This calculation gives

$$Ds = -4570\ cm^{-1}, \qquad Dt = -143\ cm^{-1}$$

These values are much larger than the values $Ds = -177\ cm^{-1}$, $Dt = -33\ cm^{-1}$ for tetragonal cobaltous oxide. This shows that a rather exaggerated tetragonal distortion is present in VO^{++} complex.

III. MOLECULAR ORBITAL METHOD

Ballhausen and Gray noticed that the small value of Dq can be explained by considering the π bonding between the V^{4+} ion and the vanadyl oxygen.

We will take the 3d, 4s, and 4p orbitals of metal ion, the 2s, $2p_\sigma$, and $2p_\pi$ orbitals of vanadyl oxygen, and the sp_σ hybrid orbitals of the water oxygens to construct the molecular orbitals. The transformation scheme of these orbitals in C_{4v} is given in Table II. The ligands are numbered as shown in Fig. 1. We combine the atomic orbitals (or the combination of those

TABLE II

TRANSFORMATION SCHEME OF ORBITALS OF METAL ION, VANADYL OXYGEN, AND WATER OXYGEN

Representation	Metal Orbitals	Ligand Orbitals
a_1	$4s, 4p_z, 3d_{z^2}$	$\sigma_5, \sigma_6, \frac{1}{2}(\sigma_1+\sigma_2+\sigma_3+\sigma_4)$
b_1	$3d_{x^2-y^2}$	$\frac{1}{2}(\sigma_1-\sigma_2+\sigma_3-\sigma_4)$
b_2	$3d_{xy}$	
e	$3d_{xz}, 3d_{yz}, 4p_x, 4p_y$	$\pi_5(2p_x, 2p_y), \frac{1}{\sqrt{2}}(\sigma_1-\sigma_3), \frac{1}{\sqrt{2}}(\sigma_2-\sigma_4)$

orbitals) χ_k belonging to the same representation to get the molecular orbitals, i.e.,

$$\phi_i = \sum_k \chi_k C_{ki} \qquad (1)$$

The orbital energies and the constant coefficients C_{ki} can be obtained by variational method.

Introduce matrix notations for the set of atomic orbitals belonging to the same representation, and the coefficients

$$\mathcal{X} = (\chi_1, \chi_2 \cdots\cdots \chi_m)$$

$$C_i = \begin{pmatrix} C_{1i} \\ C_{2i} \\ \vdots \\ C_{mi} \end{pmatrix}$$

Then Eq. (1) for the ith MO can be rewritten as

$$\phi_i = \mathcal{X} C_i \tag{2}$$

and the energy of this orbit is

$$E = \int \bar{\phi}_i \mathcal{H} \phi_i d\tau = C_i^* \mathcal{H} C_i \tag{3}$$

where $\mathcal{H}$ is the Hamiltonian of an electron in the field of all the nuclei in the complex, and $\mathcal{H}$ is a matrix with elements

$$(\mathcal{H})_{pq} = \int \bar{\chi}_p \mathcal{H} \chi_q d\tau \tag{4}$$

The normalization condition ($\int \bar{\phi}_i \phi_i d\tau = 1$) can be written as

$$C_i^* S C_i = 1 \tag{5}$$

where S is a matrix with elements

$$(S)_{pq} = \int \bar{\chi}_p \chi_q d\tau \qquad \text{(overlap integral)}$$

If we minimize the energy in Eq. (3) subjected to the condition in Eq. (5), we obtain, by Lagrange's method of undetermined multiplier, the following linear homogeneous equation for the coefficients C_{ki}:

$$\mathcal{H} C_i = \epsilon_i S C_i \tag{6}$$

In order to have non-trivial solutions, we must have

$$\det|\mathcal{H} - \epsilon_i S| = 0 \tag{7}$$

The orbital energy ϵ_i is obtained by solving this secular equation. The coefficients C_{ki} can be obtained by substituting the values of ϵ_i in Eq. (6).

In the so-called "semi-empirical method," the matrix elements $(\mathcal{H})_{pq}$'s are obtained from the measured VSIE (valence state ionization energy) as follows:

diagonal element $(\mathcal{H})_{pp}$ = VSIE

non-diagonal element $(\mathcal{H})_{pq} = -2(S)_{pq}\sqrt{(\mathcal{H})_{pp}(\mathcal{H})_{qq}}$

Since the VSIE's for the different atoms vary considerably with the degree of ionization, a charge distribution for $VO(H_2O)_5^{++}$ must be assumed for the initial calculation. After computing the coefficients, the charge distribution is calculated as follows.[10]

Let the ith MO be

$$\phi_i = \sum_{r,k} C^i_{r,k}\, \chi_{r,k}$$

where the subscripts r,k refer to the rth AO on kth atom. Take the absolute

value square

$$|\phi_i|^2 = \sum_{r,k} |C^i_{r,k}|^2 |\chi_{r,k}|^2 + \sum_{r,k \neq s,\ell} \overline{C}^i_{r,k} C^i_{s,\ell}\, \overline{\chi}_{r,k} \chi_{s,\ell}$$

Multiply by the number of electrons in this orbital n_i, and integrate over all space; then

$$n_i = n_i \sum_{r,k} |C^i_{r,k}|^2 + n_i \sum_{r,k \neq s,\ell} \overline{C}^i_{r,k} C^i_{s,\ell}\, S_{rks\ell}$$

where $S_{rks\ell}$ is the overlap integral between $\chi_{r,k}$ and $\chi_{s,\ell}$.

Define various electron populations as follows:

AO population $N(i,rk) = n_i |C^i_{r,k}|^2 + n_i C^i_{r,k} \sum'_{s\ell(\neq rk)} C^i_{s,\ell} S_{rks\ell}$

MO population $N(i,k) = \sum_r N(i,rk)$

Atomic population $N(k) = \sum_i N(i,k)$

The gross charge (in unit +e) on any atom can be defined as

$$Q(k) = N_o(k) - N(k)$$

where $N_o(k)$ is the total number of electrons in the ground state of the free neutral atom.

This procedure is repeated until a self-consistent answer appears. The final charge distribution is

$$V^{+0.97}O^{-0.60}(5H_2O)^{+1.63}$$

The result of Ballhausen and Gray's calculation of energy level is shown in Fig. 3.

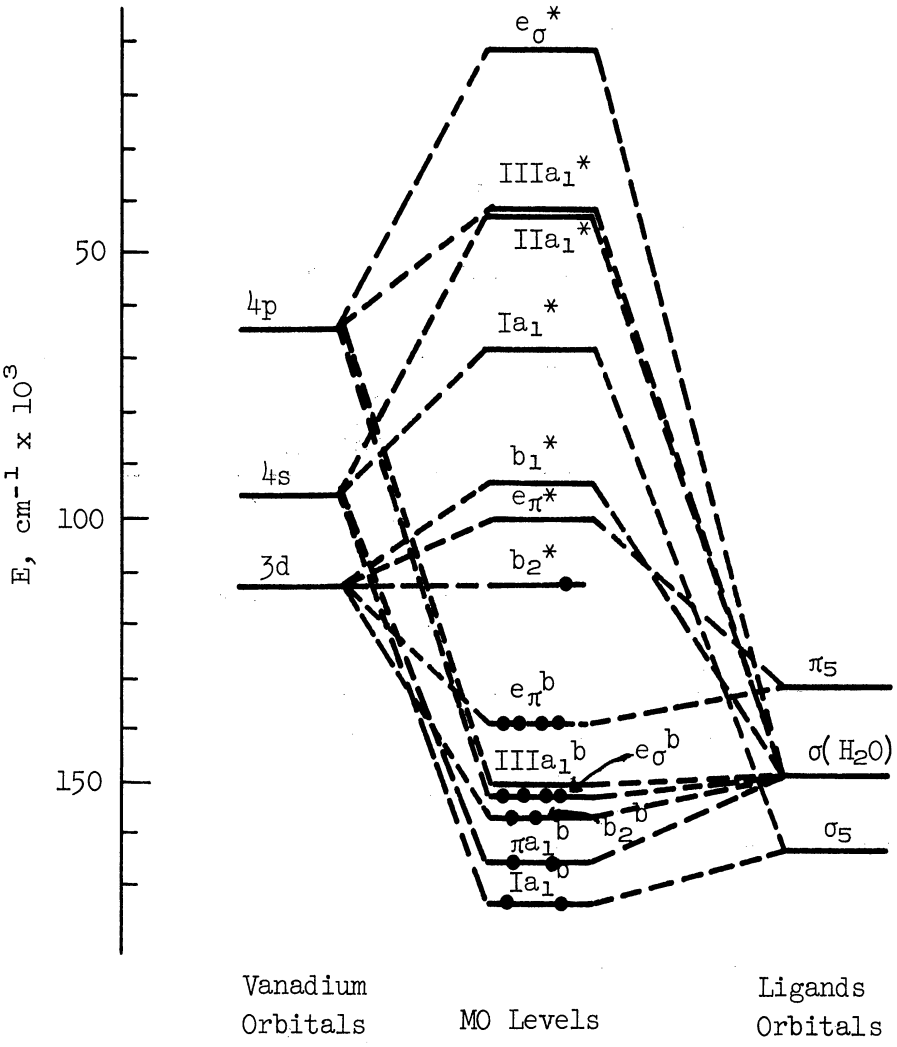

Fig. 3. Molecular orbital scheme for $VO(H_2O)_5^{++}$. The levels are drawn to scale.

There are 17 electrons (12 from 6 ligand σ orbitals, 4 from oxygen π orbitals and 1 from V^{4+}) to be placed in these orbitals. Thus the ground state configuration

$$(Ia_1^b)^2(IIa_1^b)^2(b_1^b)^2(e_\sigma^b)^4(IIIa_1^b)^2(e_\pi^b)^4(b_2)^1$$

is a $^2B_2$.

The so-called crystal field transitions involve moving the b_2 electron

to the antibonding e_π^*, b_1^* and Ia_1^* MO's, resulting in $^2E(I)$, $^2B_1$, and $^2A_1$ excited states respectively (see Table III).

TABLE III

SPECTRUM OF $VOSO_45H_2O$

Band Type	Transition	Predicted Energy and Polarization		Observed Energy and Polarization	
Crystal Field	$^2B_2 \rightarrow {}^2E(I)$	12,502 cm^{-1}	($\perp$)	13,060 cm^{-1}	($\perp$)
	$^2B_2 \rightarrow {}^2B_1$	18,794	(all)	16,000	(all)
	$^2B_2 \rightarrow {}^2A_1$	44,766	(all)	Covered	
Charge Transfer	$^2B_2 \rightarrow {}^2E(II)$	38,8000	($\perp$)	41,700	($\perp$)
	$^2B_2 \rightarrow {}^2B_2$	44,000	($\parallel$)	50,000	($\parallel$)

Since the electric dipole vectors transform as $A_1(z)$ and $E(x,y)$ in C_{4v}, only transitions to $B_2(=B_2 \times A_1)$ and $E(=B_2 \times E)$ are orbitally allowed. Thus the transition $^2B_2 \rightarrow {}^2E$ must have the greatest intensity and is polarized perpendicular to VO axis (z axis). The other two transitions are allowed vibronically and should appear in all polarization.

One of the charge transfer bands is due to the promotion of an electron from the e_π^b orbital to the b_2 orbital, resulting in the configuration

$$^2E(II)\,[(\text{inner core})^{12}(e^b)^3(b_2)^2]$$

Another charge transfer spectrum is due to the promotion of e_π^b electron to the e_π^* orbit: $(\text{inner core})^{12}(e_\pi^b)^3(b_2)^1(e_\pi^*)^1$. From this configuration doublet

states can be constructed that transform as A_1, A_2, B_1, and B_2 in C_{4v}. Only the transition $^2B_2 \rightarrow {}^2B_2$ is orbitally allowed.

The energies of these transitions can be predicted by adding together the orbital promotional energy and the repulsion energy contribution. (The latter is obtained from Coulomb and exchange integral.) The predicted energies are shown in Table III. Good agreement with the observed values is the result of using empirical value of VSIE.

A. g-VALUES

In the molecular orbital description, the formulae for the g-values become

$$g_{\perp} = 2\left[1 - \frac{\lambda(C_{1e}^*)^2}{\Delta E(^2B_2 \rightarrow {}^2E)}\right]$$

$$g_{\parallel} = 2\left[1 - \frac{4\lambda(C_{1b}^*)^2}{\Delta E(^2B_2 \rightarrow {}^2B_1)}\right]$$

where C_{1e}^* and C_{1b}^* are the coefficients of metal orbitals in the MO e_π^* and b_1^* respectively.

We can calculate g-values from these formulae using the energy values obtained above and the spin-orbit coupling constant $\lambda = 135$ cm^{-1}. (Since the charge on vanadium is +0.97, the value of λ for V^+ is used.[11] The result of calculation is shown in Table IV, along with some experimental results for comparison.

TABLE IV

CALCULATION OF g-VALUES

g	Calculated	Exp., Aqueous Solution	Exp., Powder[12]
$g_{\parallel}$	1.940		1.9328±2
$g_{\perp}$	1.983		1.9802±3
<g>	1.969	1.962	1.9644±3

B. DERIVATION OF THE FORMULAE FOR g-VALUES

Let the wave functions of the MO b_2, e_π^*, and b_1^* be

$$|b_2\rangle : \frac{1}{\sqrt{2}}(Y_{22}-Y_{2\bar{2}})$$

$$|e_\pi^*\rangle : C_{1e}^* \frac{1}{\sqrt{2}}(Y_{21}-Y_{2\bar{1}}) + C_{2e}^* \frac{1}{\sqrt{2}}(Y_{11}-Y_{1\bar{1}}) \qquad (=C_{1e}^*|xz\rangle + C_{2e}^*|x\rangle)$$

$$|b_1^*\rangle : C_{1b}^* \frac{1}{\sqrt{2}}(Y_{22}+Y_{2\bar{2}}) + C_{2b}^* \frac{1}{2}(\sigma_1-\sigma_2+\sigma_3-\sigma_4) .$$

If magnetic field H||z, the perturbation Hamiltonian

$$\mathcal{H}_{\parallel} = \lambda L\cdot S + \beta H(L_z+2S_z) .$$

Then

$$\langle b_2|\mathcal{H}_{\parallel}|b_2\rangle = 2\beta H S_z$$

$$\langle e_\pi^*|\mathcal{H}_{\parallel}|b_2\rangle = \lambda C_{1e}^* S_x$$

$$\langle b^*|\mathcal{H}_{\parallel}|b_2\rangle = 2C_{1b}^*(\lambda S_z+\beta H) .$$

By 2nd order perturbation:

$$E_{\parallel}' = 2\beta HS_z - \frac{|\langle e_\pi^* | \mathcal{H}_{\parallel} | b_2 \rangle|^2}{\Delta E(b_2 \to e_\pi^*)} - \frac{|\langle b_1^* | \mathcal{H}_{\parallel} | b_2 \rangle|^2}{\Delta E(b_2 \to b_1^*)}$$

$$= 2\beta HS_z - \frac{8(C_{1b}^*)^2 \lambda \beta HS_z}{\Delta E(b_2 \to b_1^*)} + O(H^2, \lambda^2)$$

$$= g_{\parallel} \beta H \cdot S_z$$

Therefore

$$g_{\parallel} = 2 - \frac{8(C_{1b}^*)^2 \lambda}{\Delta E(b_2 - b_1^*)}$$

If magnetic field $H \perp z$ (e,g., $H \| x$), the perturbation Hamiltonian

$$\mathcal{H}_{\perp} = \lambda L \cdot S + \beta H(L_x + 2S_x) \ .$$

Then

$$\langle b_2 | \mathcal{H}_{\perp} | b_2 \rangle = 2\beta HS_x$$

$$\langle b_1 | \mathcal{H}_{\perp} | b_2 \rangle = 2\lambda S_z C_{1b}^*$$

$$\langle e_\pi^* | \mathcal{H}_{\perp} | b_2 \rangle = C_{1e}^*(\beta H + \lambda S_x)$$

By 2nd order perturbation:

$$E_{\perp}' = 2\beta HS_x - \frac{(C_{1e}^*)^2(\beta H + \lambda S_x)^2}{\Delta E(b_2 \to e_\pi^*)} - \frac{(C_{1b}^*)^2(2\lambda S_z)^2}{\Delta E(b_2 \to b_1)}$$

$$= 2\beta HS_x - \frac{2(C_{1e}^*)^2 \lambda \beta HS_x}{\Delta E(b_2 \to e_\pi^*)} + O(H^2, \lambda^2)$$

$$= g_{\perp} \beta HS_x$$

Therefore

$$g_{\perp} = 2 - \frac{2(C_{1e}^{*})^{2}\lambda}{\Delta E(b_{2}-e_{\pi}^{*})} \quad .$$

IV. REFERENCES

1. Griffiths *et al.*, Proc. Roy. Soc. (London) A219, 529 (1953).
2. Griffiths *et al.*, Proc. Roy Soc. (London) A226, 96 (1954).
3. Tinkham, Proc. Roy. Soc. (London) A236, 535 and 549 (1956).
4. Parr and Mulliken, J. Chem. Phys. 18, 1338 (1950).
5. Crawford and Parr, J. Chem. Phys. 17, 726 (1949).
6. Crawford and Parr, Trans. Faraday Soc. 49, 1 (1953).
7. Ellison and Shull, J. Chem. Phys. 21, 1420 (1953).
8. Wolfsberg and Helmholz, J. Chem. Phys. 20, 837 (1952).
9. Ballhausen and Gray, Inorg. Chem. 1, 111 (1962).
10. Mulliken, J. Chem. Phys. 23, 1833 (1955).
11. Dunn, Trans. Faraday Soc. 57, 1441 (1961).
12. Result obtained in our laboratory by R. H. Borcherts.

PART C

OPTICAL PROPERTIES OF NUCLEAR RECOIL DEFECTS IN CADMIUM SULFIDE

by

Robert B. Oswald, Jr.

I. OBJECTIVES

The objectives of this study are to determine experimentally the changes in the optical properties of crystalline cadmium sulfide produced by nuclear recoil of Cd^{114} and to determine a model which fully describes these optical effects. To determine the changes produced by the recoil of Cd^{114} it is anticipated that the following measurements will be made:

(A) Luminescence under U.V. excitation

(B) Absorption

(C) Photoconductivity

(D) Infrared quenching

Since the use of Cd^{114} recoil is a unique means of producing cadmium defects in the CdS host crystal, this study will also lead to a greater understanding of the optical properties of solids and their relationship to vacancy and interstitial defects.

II. OPTICAL PROPERTIES OF Cd DEFECTS BY NUCLEAR RECOIL

A. PRODUCTION OF DEFECTS BY Cd^{114} RECOIL

There are many ways of producing defects in the crystalline structure of CdS, such as electron bombardment, proton bombardment, γ radiation, heat treatment in special environments, fast neutron bombardment, and the recoil of a nucleus due to the emission of particles or γ rays. But of these methods only one, the method of nuclear recoil, provides an unambiguous identification of the constituent producing the defect and the types of defects being produced. In this study, therefore, the method used to produce cadmium interstitial and vacancy defects in CdS is nuclear recoil of Cd^{114}.

To create both cadmium interstitial and vacancy defects, samples of cadmium sulfide are irradiated with thermal neutrons. The basic mechanism which produces these defects is the recoil of Cd^{114} through the emission of prompt γ's in the reaction

$$Cd^{113} + n_{th} \rightarrow Cd^{114} + \gamma \qquad E\gamma = 9 \text{ mev}$$

where the recoil energy of the Cd nucleus is given by

$$E_{Cd\ recoil} = \frac{E\gamma^2}{2mC^2} = \frac{E\gamma^2(mev)}{2.12 \times 10^5} \qquad \text{in mev}$$

As shown in Table I, natural cadmium contains 12.3% Cd^{113}, which has a thermal neutron absorption cross section that is four orders of magnitude greater than the cross sections of the other naturally occurring isotopes of cadmium and sulfur. Thus it is evident that the dominant effect of thermal neutron

irradiation will be the creation of Cd^{114} through the $Cd^{113}(n,\gamma)$ Cd^{114} reaction. Furthermore, both cadmium vacancy and interstitial defects will be produced by the nuclear recoil of Cd^{114}, provided the recoil energy is greater than the minimum energy required for displacement.

TABLE I

ISOTOPIC CONSTITUENTS OF CADMIUM AND SULFUR

Element	Isotopic Constituents	% Abundance	Thermal Neutron Absorption Cross Section, Barns
Cd	Cd^{106}	1.215	1.0
	Cd^{108}	0.875	---
	Cd^{110}	12.39	0.02
	Cd^{111}	12.75	---
	Cd^{112}	24.07	0.03
	Cd^{113}	12.26	20,000.
	Cd^{114}	28.76	1.14
	Cd^{116}	7.58	1.5
S	S^{32}	25.0	0.002
	S^{33}	0.76	0.015
	S^{34}	4.22	0.26
	S^{36}	.014	0.14

Although the minimum displacement energy as determined by electron bombardment is approximately 8 ev, the above proviso cannot be fully eliminated since the 9-mev γ energy appears in a cascade of many γ's whose spectrum and angular correlation has not been completely determined. Although the efficiency of this defect-producing mechanism cannot be explicitly evaluated, it can be shown to be greater than zero, and hence a means of producing both cadmium vacancies and interstitial defects.

B. OPTICAL PROPERTIES OF Cd DEFECTS

As mentioned above, the recoil of a Cd^{114} nucleus from its lattice position will result in the production of both cadmium vacancy and interstitial sites. It is anticipated that both of these defects may have energy levels which lie in the forbidden gap of the crystal's band structure.

Thus, through the irradiation of CdS by thermal neutrons we will produce either new levels in the forbidden energy gap or increase the density of existing levels. Since the absorption, luminescence, photoconductivity, and infrared quenching of this crystal are directly related to its electron energy band structure, measurements of these optical properties and their changes due to Cd^{114} recoil will enable us to construct a band model which effectively describes these sites.

III. PRESENT STATUS

To date emphasis has been placed upon the construction of a fluorescence spectrometer and on the production of effects on the luminescence and conductivity properties of cadmium sulfide crystals due to Cd^{114} recoil.

The fluorescence spectrometer is being constructed to enable us to measure the luminescence spectra of the CdS samples before and after irradiation. A schematic diagram of the instrument is shown in Fig. 1.

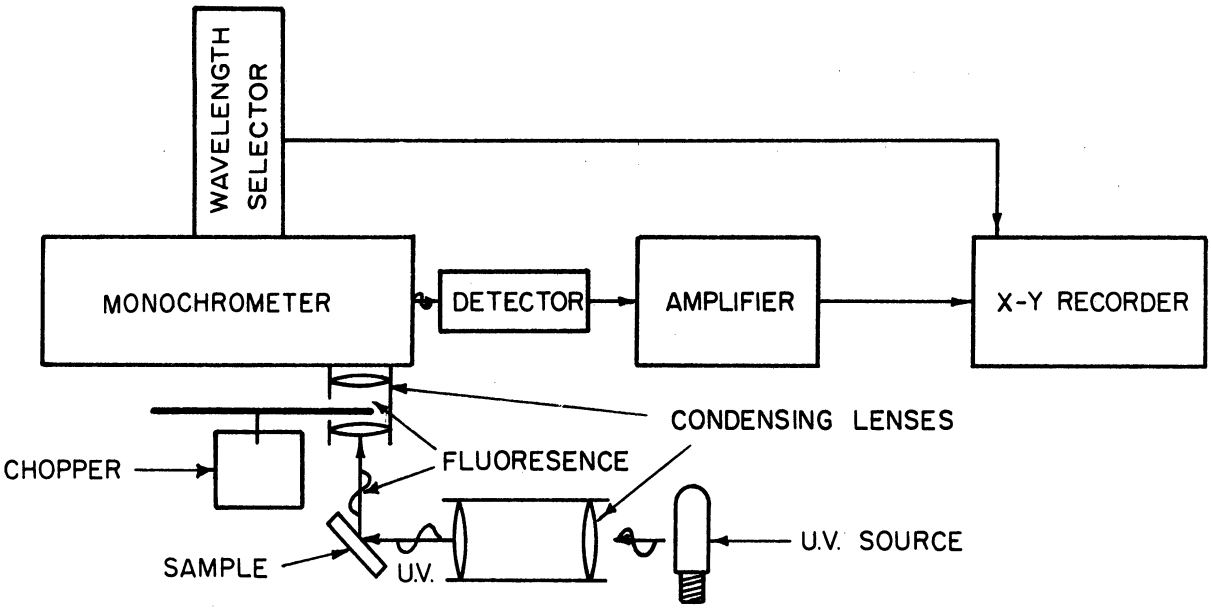

Fig. 1. Schematic diagram of the fluorescence spectrometer.

The instrument has been developed to the state where it will observe the spectra of luminescent samples. However, in the red region of the spectra its sensitivity is still too low to make it usable. Steps are currently being taken to improve its performance by (1) increasing the U.V. intensity, (2) increasing the resolution of the monochromator, (3) increasing the sensitivity

of the detector, and (4) increasing the noise rejection capabilities of the amplifier.

The preliminary results which have been obtained to date are exciting. Samples of cadmium sulfide have been irradiated in the Ford Nuclear Reactor, producing definite changes in their luminescence and photoconductivity properties. Moreover, these effects are the result of defects produced by thermal neutrons, which indicates that they are the result of Cd^{114} recoil. The specific results are discussed below.

A. NEUTRON IRRADIATION OF SAMPLES

To produce cadmium defects in the cadmium sulfide crystals the samples were irradiated with neutrons using pneumatic tube No. 4 of the Ford Nuclear Reactor. The samples were first placed in a "rabbit," which acts as a carrier, and were then inserted into the pneumatic tube system which brings the sample to a position approximately 6 in. from the core.

All of the samples observed to date have been irradiated for 1 hr at a power level of 1 mw. When the reactor is operating at this power level, the neutron flux at the "rabbit" is approximately 10^{11} neutrons/cm^2 sec and 10^{12} neutrons/cm^2 sec for thermal and fast neutrons respectively.

The identical appearance of these crystals before and after irradiation is an indication that the basic structure of the crystal has not been destroyed in the process.

To distinguish between the thermal neutron effect and the fast neutron effect, samples were irradiated both with and without a cadmium cover. The

cadmium cover consisted of a cadmium metal sheath 40 mils thick, which effectively eliminates thermal neutrons from the sample.

B. LUMINESCENCE

To observe the changes in the luminescence properties of crystalline cadmium sulfide, several samples of single crystal CdS were irradiated with both fast and thermal neutrons as described above. Before neutron irradiation these samples showed little or no fluorescence at liquid nitrogen temperature under U.V. excitation. However, after irradiation all these samples fluoresced red at liquid nitrogen temperature under U.V. excitation. The luminescence spectrum of one of these samples showed that neutron irradiation had produced a broad red band centered at 7200A.

To evaluate whether or not this was a thermal neutron effect, cleaved mates of these samples were irradiated with 40-mil cadmium covers, thus eliminating the thermal neutrons.

After irradiation none of the samples fluoresced with the characteristic red of the uncovered sample. Hence we can conclude that the change in the luminescence is the result of thermal neutrons.

Further experiments have been carried out to ensure that this change in the luminescence spectrum is not the result of the production of an interstitial cadmium atom and subsequent oxidation. Two tests were designed: the first was an annealing experiment and the second was irradiation of the sample sealed in a helium-filled quartz ampule.

The theory on which the first test was based is that if the cadmium interstitials had combined with oxygen, the red luminescence would not show an

annealing effect. This check was carried out by first measuring the red luminescence spectrum of one sample. This sample was then sealed in a quartz ampule filled with helium. The annealing was then carried out by heating this ampule to 500°C and holding for 5 hr. Upon cooling, the red spectrum of this sample was again measured. The result of this measurement showed that the intensity of the red luminescence had decreased below a detectable level. Thus, by the annealing test it appears that this is not an oxidation effect.

The second test, in which the sample is irradiated in a helium atmosphere, is currently being carried out. A fluorescence spectrum of the sample has been measured and the sample then sealed in a helium-filled quartz ampule. The sample was irradiated for 1 hr at 1 mw and is still too "hot" for examination of its fluorescence spectrum.

C. CONDUCTIVITY

In addition to the production of a broad red luminescence band, large changes in the conductivity of these crystals have been produced by thermal neutrons. Several samples of single crystal CdS which were conducting at room temperature were irradiated in the reactor as described above. Irradiations were done both with and without cadmium covers over the crystals in order to evaluate the thermal neutron effect. The results of these measurements are shown in Tables II and III.

As shown in these two tables, irradiation by both fast and thermal neutrons produces a large decrease in the conductivity, whereas irradiation

TABLE II

CHANGES IN CONDUCTIVITY OF CdS CRYSTALS DUE TO IRRADIATION BY FAST AND THERMAL NEUTRONS

Sample No.	Conductivity Before Irradiation		Conductivity After Irradiation	
	In Room Light	Dark	In Room Light	Dark
29^{I}	30.0×10^{-3} mhos	30.0×10^{-3} mhos	8.3×10^{-3} mhos	8.0×10^{-3} mhos
26^{I}	7.3×10^{-3} mhos	7.3×10^{-3} mhos	2.2×10^{-3} mhos	1.56×10^{-3} mhos
32^{I}	9.0×10^{-3} mhos	9.0×10^{-3} mhos	1.7×10^{-3} mhos	1.25×10^{-3} mhos

TABLE III

CHANGES IN CONDUCTIVITY OF CdS CRYSTALS DUE TO IRRADIATION BY FAST NEUTRONS

Sample No.	Conductivity Before Irradiation		Conductivity After Irradiation	
	In Room Light	Dark	In Room Light	Dark
29^{II}	40.0×10^{-3} mhos	40.0×10^{-3} mhos	35.0×10^{-3} mhos	35.0×10^{-3} mhos
26^{II}	7.8×10^{-3} mhos	7.8×10^{-3} mhos	7.7×10^{-3} mhos	7.7×10^{-3} mhos

by fast neutrons does not. Hence it is evident that the decrease in conductivity is due to thermal neutrons. In addition it is evident that the conductivity of the crystals irradiated by thermal neutrons becomes light-sensitive. One interpretation of these results is that thermal neutron irradiation produces an electron trap since the conductivity of CdS is largely due to electrons. The effect of these traps is to reduce the conductivity by trapping electrons from the conduction band. Furthermore, the increase in conductivity

under illumination by room light is due to the excitation of these trapped electrons into the conduction band.

IV. FUTURE PLANS

These preliminary results show that undoubtedly we have produced defects in cadmium sulfide crystals due to thermal neutrons which change the optical properties of the crystal. Hence we are embarking upon a program to measure the optical properties and their changes due to thermal neutron irradiation as outlined in Section II. The objective of this program will be to produce a model which fully describes these effects.